

**NASA TECHNICAL
MEMORANDUM**



NASA TM X-3335

NASA TM X-3335

**CASE FILE
COPY**

**EFFECTS OF PERFORATED FLAP SURFACES
AND SCREENS ON ACOUSTICS OF A LARGE
EXTERNALLY BLOWN FLAP MODEL**

*Robert J. Burns, Daniel J. McKinzie, Jr.,
and Jack M. Wagner*

*Lewis Research Center
Cleveland, Ohio 44135*



1. Report No. NASA TM X-3335	2. Government Accession No.	3. Recipient's Catalog No.	
4. Title and Subtitle EFFECTS OF PERFORATED FLAP SURFACES AND SCREENS ON ACOUSTICS OF A LARGE EXTERNALLY BLOWN FLAP MODEL		5. Report Date April 1976	6. Performing Organization Code
		8. Performing Organization Report No. E-8559	10. Work Unit No. 505-03
7. Author(s) Robert J. Burns, Daniel J. McKinzie, Jr., and Jack M. Wagner		11. Contract or Grant No.	
		13. Type of Report and Period Covered Technical Memorandum	
9. Performing Organization Name and Address Lewis Research Center National Aeronautics and Space Administration Cleveland, Ohio 44135		14. Sponsoring Agency Code	
		12. Sponsoring Agency Name and Address National Aeronautics and Space Administration Washington, D.C. 20546	
15. Supplementary Notes			
16. Abstract Various model geometries and combinations of perforated flap surfaces and screens mounted close to the flap surfaces were studied for application to jet-flap noise attenuation for externally blown flap, under-the-wing aircraft. The efforts to reduce jet-flap interaction noise were marginally successful. Maximum attenuations of less than 4 dB in overall sound pressure level were obtained in the flyover plane. Noise reductions obtained in the low- to middle-frequency ranges (up to 7 dB) were generally offset by large increases in high-frequency noise (up to 20 dB).			
17. Key Words (Suggested by Author(s)) Jet aircraft noise Jet impingement Short takeoff aircraft Noise suppression		18. Distribution Statement Unclassified - unlimited STAR Category 02 (rev.)	
19. Security Classif. (of this report) Unclassified	20. Security Classif. (of this page) Unclassified	21. No. of Pages 40	22. Price* \$3.75

* For sale by the National Technical Information Service, Springfield, Virginia 22161

EFFECTS OF PERFORATED FLAP SURFACES AND SCREENS ON ACOUSTICS OF A LARGE EXTERNALLY BLOWN FLAP MODEL

by Robert J. Burns, Daniel J. McKinzie, Jr., and Jack M. Wagner

Lewis Research Center

SUMMARY

Several potential means for reducing the jet-flap interaction noise of externally blown flap, under-the-wing configurations were investigated acoustically by using a large-scale, two-flap model with a conical nozzle (33 cm diam). Initially, perforated surfaces were used in various combinations and porosities on the flap leading and trailing edges. Tests then were made of the ability of various-size screens mounted close to the flap surfaces to attenuate flap noise. Finally, combinations of perforated flap surfaces and screens were tested. In general, the acoustic data showed that on the basis of overall sound pressure level, a maximum attenuation of less than 4 decibels could be achieved in the flyover plane. This attenuation was achieved with a combined perforated-surface-and-screen configuration. On the basis of spectral data, the devices used tended to reduce the noise level in the middle-frequency range (400 to 2000 Hz) by as much as 7 decibels. However, this attenuation was offset by as much as 20 decibels increase in noise at high frequencies ($>10\ 000$ Hz). None of the efforts to reduce the jet-flap interaction noise were significantly effective over the entire frequency range. Scaling of the present acoustic attenuation results to a full-size aircraft could produce adverse effects in the most annoying region of the jet-flap noise spectrum. In addition, the marginal acoustic benefits of the attenuation devices would be offset by inherent penalties in weight, lift, drag, and structural complexity.

INTRODUCTION

The nature of the operation of powered-lift aircraft, as well as the possibility of more restrictive noise goals, requires that powered-lift aircraft be considerably quieter than conventional (CTOL) aircraft (refs. 1 to 3). For the engine-under-the-wing (UTW), externally blown flap (EBF) concept of powered lift, shown schematically in figure 1, the jet-flap interaction noise is the dominant aircraft noise source. Previous tests of

powered-lift aircraft using conventional (solid) flap surfaces (e. g. , ref. 4) resulted in jet-flap interaction noise that was 15 to 30 decibels above the suggested requirement of 95 EPNdB at 152.4 meters.

In reference 4, using a small-scale three-flap system, Hayden suggests that the primary noise sources of jet-flap interaction are at the leading and trailing edges of the flaps deployed for takeoff or landing. Hayden says, "the dipole-like sound from jet interaction with the flaps and their edges dominates the sound output from a subsonic jet/deployed flap system." The small-scale studies of reference 4 also showed that the use of perforated flap surfaces could reduce the jet-flap interaction noise 10 decibels by modifying the acoustics associated with edge noise. Another means for accomplishing a noise reduction of 10 decibels was through the use of a screen between the nozzle exhaust plane and the flap surfaces. The screen modified the turbulence structure and intensity of the jet flow impinging on the flap surfaces. The aerodynamic penalties associated with the use of perforated flap edges and screen coverings over the impingement surface were also measured in reference 4. Lift losses for both the takeoff and approach flap settings were of the order of 10 to 25 percent. Drag increases were observed to be 15 and 40 percent for the approach setting and 40 and 100 percent for the takeoff setting.

In the present work, various noise suppression means, many similar to those used in reference 4, were evaluated acoustically with a large-scale EBF-UTW configuration because it was believed that direct scaling laws might not apply. A two-flap wing model with a conical nozzle (33 cm diam) that is representative of designs being considered for use with STOL (short takeoff and landing) aircraft was used in the test program. The leading- and trailing-edge sections of both flaps were modified by substituting perforated skins for solid skins. One-piece perforated skins were wrapped around both the pressure and suction surfaces of the flaps for a distance approximately equal to 25 percent of the flap chord length. Several perforated-skin porosities (defined by percentage of open area) were tested. The data were neither optimized as to the size of holes required in the perforated skin nor as to the number of holes or the spacing feasible for EBF applications. In addition, configurations with wire fabric screens installed near the surface of the underside of the flaps were tested. The effect on acoustics of reducing the flap-slot spacing was also investigated.

Data were recorded at nozzle jet velocities of 166, 228, and 258 meters per second with a 60° total deflected flap landing configuration. The far-field acoustics, the flap surface pressures, and the velocity profile were measured at the trailing edge of the second flap. In this report, typical acoustic characteristics at the 85° flyover angle are shown for the many flap-treatment configurations; however, data at other directivity angles are also included. Lift and drag were not measured in the present study because reference 4 includes a sufficient amount of such data to yield estimates for most of the configurations used herein. All symbols are defined in the appendix.

APPARATUS AND PROCEDURE

Test Facility

The test facility is an outdoor structure with provisions for attaching a wing segment so that the jet centerline is 3.89 meters above a hard macadam surface (fig. 2). The exhaust nozzle was supplied with ambient dry air from the NASA Lewis Research Center's propulsion air supply system ($1.03 \times 10^6 \text{ N/m}^2 \text{ max}$). The air was brought to the test site through a 61-centimeter-diameter underground line. An orifice flowmeter was located in a straight section of the underground line upstream of a 40.7-centimeter-diameter gate shutoff valve at the test site. The EBF test-facility flow system, shown in figure 2, was connected to the gate valve. Two flow distribution and quieting screens were located between the last elbow of the test-facility flow system and the nozzle assemblies. The supply system noise suppression was provided by extensive internal and external treatment, as described in reference 3.

The operating pressure ratio (nozzle total pressure divided by ambient atmospheric pressure) for the 33-centimeter-diameter convergent nozzle was set by the flow control valve and supply pressure.

Nozzle total pressures and temperatures were measured at the nozzle inlet downstream of the screens. The nozzle jet exhaust velocities V_N were determined from the fully expanded isentropic equations.

Model Configurations

The EBF-UTW model used in these tests and shown in figures 2 and 3 was similar to that described in reference 5. The EBF model was mounted with the 2.74-meter-span wing section in a vertical position with the axis of the nozzle located 3.89 meters above grade. The exhaust plane of the 33-centimeter-diameter conical nozzle was 38.1 centimeters ahead of the wing leading edge. The nozzle centerline (axis) was located at a spanwise position 1.52 meters from the bottom of the wing section and 1.22 meters from the top.

The straight two-dimensional wing section of the basic model had a nominal chord length of 2.08 meters with the flaps retracted. In the present investigation, the two-flap system was tested with the flaps in the landing setting (last flap deflected 60° to the wing chord), as shown in figure 3. The flap cross sections and coordinates are given in figure 4. The cavities shown in figure 4 were sized for structural considerations, and the Helmholtz effects were not determined.

Hard-wall baseline configuration. - The baseline configuration differed from the EBF model of reference 5 in the gap between the center flap sections and in chord size.

Generally, the present baseline configuration had a gap of 5.8 centimeters (fig. 5) compared with 4.3 centimeters for the model of reference 5. The flap chords were also slightly shorter in the present model (fig. 5) than those used in reference 5. The gap between the center flap sections was made equal to that of the outer flap sections (4.3 cm) during part of this test in order to determine the effect of gap size on the noise.

Perforated flap surfaces. - Representative treated flap configurations are shown in figure 6. As shown, it was necessary to treat the flap leading and trailing edges only along the span of the wing on which high-velocity gas impinges.

Cross sections and dimensions of the flaps that were used with perforated surfaces are shown in figure 4. The cross-hatched center region denotes a sealed section. The leading- and trailing-edge cavities were divided into eight compartments along the span, each approximately 14.6 centimeters wide and 14.6 centimeters long (25 percent of the local chord). Various perforated surfaces were attached over the leading- and trailing-edge cavities. Three surface porosities were evaluated: 4, 15, and 44 percent open area. The surfaces were fabricated from commercial aluminum or stainless-steel perforated sheet. Scottfelt foam was used as filler material in the leading- and trailing-edge cavities in three configurations using the 15-percent-open-area skins (table I). The geometric layouts of the perforations are shown in figure 7. The various combinations of the configurations tested are briefly described in table I. Included are the reference models, perforated-surface models, models with screens, and models with combinations of perforated skins and screens. Initially, the percentage of open area was investigated; then the treatment of the leading or trailing edges, or both; and finally combinations of the most promising perforated skins and screens. After the initial percentage-of-open-area test data were analyzed, the 15-percent-open-area skin was selected as the most acceptable aerodynamic surface for further investigation.

Flaps with screens. - The basic screened-flap configurations are shown in figure 8. Initially, large screens, each with different mesh sizes, were attached to the flow impingement side of the flaps (fig. 8(a)). The nominal screen dimensions were 1.2 by 1.2 by 0.157 centimeter (1.2 wires per cm by 1.2 wires per cm; wire diameter, 0.157 cm); 2.7 by 2.7 by 0.008 centimeter; and 11.8 by 11.8 by 0.033 centimeter. The screens were used with both hard-wall and perforated-surface flaps, as shown in table I. In addition, the standoff height of the screen from the flap surfaces was varied from 2.54 centimeters to 3.8 centimeters. Spanwise widths of the large screens used were 66 and 91.4 centimeters, depending on the particular configuration.

The ramp screen configuration shown in figure 8(b) was tested in several sizes. The spanwise widths were 66 and 91.4 centimeters; the heights varied from 2.54 centimeters to 8.9 centimeters; and the lengths were 7.6 and 17.8 centimeters. Several configurations of these ramp screens alone and with the large screens of figure 8(a) were tested (table I).

Aerodynamic Data

Cotton tufts, 7.6 centimeters long, were cemented to both flap surfaces on 7.6-centimeter centerlines in order to obtain visual evidence of the jet flow over the flaps. These tufts were distributed over a spanwise length of 1.22 meters that was centered in relation to the intersection of the jet axis with the flaps. The tuft data were obtained photographically only with the baseline hard-wall flap configuration.

Static pressure distributions over the flap surfaces were obtained with multitube plastic pressure belting attached to the flap surfaces. The locations of the static pressure taps are given in figure 9.

Velocity profile measurements normal to the surface were made on the flap pressure surface at or near the trailing edge of the second flap by a total pressure rake mounted as shown in figure 10. Surveys were made at various spanwise locations starting at the nozzle centerline position.

ACOUSTIC INSTRUMENTATION

The sound data were measured with ten 1.27-centimeter condenser microphones located 3.58 meters above the macadam surface. The microphones, equipped with wind-screens, were placed on a 15.24-meter-radius circle in a horizontal plane perpendicular to the vertically mounted wing. The center of the microphone circle was located on the nozzle centerline halfway between the nozzle exit plane and the trailing flap (fig. 11).

The sound data were analyzed on-line with an automated 1/3-octave-band spectrum analyzer. The analyzer determined sound pressure level spectra (referenced to $20 \mu\text{N}/\text{m}^2$) between 50 and 20 000 hertz for each microphone. A 4-second integration time was used. Two or three noise samples were taken at each microphone and treated analytically to reject background disturbances and random errors and to obtain an rms sound pressure level. The data were then corrected for atmospheric attenuation to give lossless data at 15.24 meters. From these sound pressure level spectra, the overall sound pressure levels were calculated for each microphone location. The data in this report do not include ground reflection corrections.

For some tests, 0.317-centimeter dynamic pressure transducers were mounted on the second flap in the locations shown in figure 12. The transducers sensed the local surface-pressure fluctuations, and their output signals were conditioned by the same equipment used for the acoustic far-field data. Thus, their output is made available in decibels.

AERODYNAMIC CHARACTERISTICS OF BASELINE FLAP CONFIGURATION

The noise characteristics of an EBF-UTW configuration are related to the impingement of the jet on the flap surfaces and the consequent flow over and around the flaps. In order to help establish the nature of the present flap-system aerodynamics, visual flow studies were made, the pressure distribution about the flap surfaces was determined, and jet velocity profile surveys at the second-flap trailing edge were made. The following sections contain the results of these studies.

Visual Flow Study

Typical flow patterns over the flap surfaces, as determined by tuft studies, are shown in figure 13 for a jet velocity of 228 meters per second. The flow over the impact (lower) surface of the second flap (fig. 13(a)) is stable and well defined. However, the tufts indicate that the flow over the impact (lower) surface of the first flap had a periodic reverse flow component near the flap surface in the vicinity of the flow field's centerline. At all jet velocities (166, 228, and 258 m/sec), a wavelike action, illustrated by reversals in the tuft pattern to the mean flow direction, took place over the entire chordwise extent of the first flap. This indicates that the flow field was unstable and was periodically separating in the concave section of the flap, starting at approximately 50 percent of the flap's chord and extending to its trailing edge. The period of this reversal was about 2 seconds.

Tufts on the suction (upper) surfaces of the flaps (fig. 13(b)) indicated that the flow over the second flap was stable, whereas the flow over the first flap was unattached (being outside the flow field).

Flap Pressure Distribution

Representative steady-state pressure coefficients C_p for the second flap of the baseline configuration are shown in figure 14 as a function of distance along the flap surfaces. These data indicate that the flow field around the second flap is attached on both its upper and lower surfaces.

According to the pressure data, the flow over the suction (upper) surface of the first flap was detached, and the flow over its impact (lower) surface was poorly attached and weak. Thus the first flap was ineffective aerodynamically, and these results substantiate the observation made from the tuft study.

Trailing-Edge Velocity Survey

In figure 15 the velocity profiles for the impact (lower) surface at the trailing edge of the second flap are shown for the baseline flap configuration. The data are shown for several spanwise locations. In general, the velocity profiles are similar in shape and show the boundary layer to be very thin (i. e. , 0.5 cm). As expected the absolute values of the velocity decrease appreciably with distance from the surface and with increasing spanwise distance once the jet radius (16.5 cm) has been exceeded. (The maximum velocity is nearly equal to the jet velocity at the centerline.) A representative spanwise profile of the boundary layer velocity at a height Y of 1.1 centimeters, based on data extrapolated from figure 15, is shown in figure 16 to illustrate this point.

GENERAL ACOUSTIC RESULTS

The acoustic data presented herein show the reductions in noise levels for a large-scale EBF-UTW configuration that were obtained with the use of perforated surfaces, either as part of the flap surfaces or off the flap surfaces (screens). The data plots are presented in terms of sound pressure level (SPL) and overall sound pressure level (OASPL). Tables II and III list the more significant noise attenuations (reductions) or amplifications in terms of OASPL and SPL. The configurations are described in table I.

The data plots of OASPL and spectra, unless otherwise noted, are presented for a jet velocity of 228 meters per second and a directivity angle of 85° . This directivity angle yields representative effects of the noise attenuation associated with the various suppression means used herein for an aircraft flyover condition. Data at other directivity angles are included in tables II and III.

The variation of OASPL with jet velocity for the baseline hard-wall flap configuration varied with approximately the 5.6 power of the jet velocity. The various jet-flap interaction noise attenuation devices covered herein varied about ± 5 percent from this velocity exponent. The lowest velocity exponent (5.35) was obtained with the ramp screen plus a large impingement-area screen (configuration 17); the highest velocity exponent (5.8) was obtained by using only the large impingement-area screen (configuration 19).

In many cases the change in SPL for the various configurations compared to the baseline configuration was also a function of jet velocity, as shown in table III. This change in SPL is particularly noticeable in the high-frequency range of 4000 to 20 000 hertz. In this higher frequency range, the reductions in SPL generally increased in a negative sense with a reduction in jet velocity. In the low- and mid-frequency ranges the SPL change trend with jet velocity varied depending on the particular configuration. These increases and decreases in SPL are referenced to SPL values for the baseline

configuration operating at the same jet velocities as the configurations with the attenuation devices.

Table II does not include all the data that were taken; however, it is useful in analyzing the most effective configurations.

The following sections discuss the acoustic results from the present study in detail.

ACOUSTICS OF BASELINE HARD-WALL FLAP CONFIGURATION

Overall Sound Pressure Level

A typical variation of the OASPL with directivity angle for the baseline configuration (hard-wall flap surfaces) is given in figure 17(a). The data shown are for a jet velocity of 228 meters per second. Also shown, for comparison, are the nozzle-alone data. It is apparent that, with a wing-flap system, the noise is significantly greater than with the nozzle alone. For this jet velocity, the greatest increase in OASPL with the wing-flap system, up to about 20 decibels, occurred in the forward quadrant at directivity angles of 10° to 70° . The increase in OASPL thereafter decreased with directivity angle, reaching +10 decibels at a microphone radial angle θ of 115° . Comprehensive acoustic data for the baseline configuration are also given in references 1 to 3 and 5 to 7.

Spectra

For an overall flap deflection angle of 60° , which represents the landing condition, the directivity angle of 85° probably represents the direction closest to directly below the aircraft. According to figure 17(a), for example, the angular range directly below the aircraft gives approximately a near-maximum OASPL increase because of the jet-flap interaction noise.

For the baseline configuration the spectrum at a directivity angle of 85° is shown in figure 17(b) in terms of SPL as a function of frequency. The data shown are for a jet velocity of 228 meters per second. Also shown in the figure, for comparison, are the SPL data for the nozzle alone. The SPL for the EBF-UTW configuration is greater than that for the nozzle alone over the entire frequency range. This difference in SPL varies from nearly 20 decibels at the lower frequencies to 10 decibels at the highest frequencies for this jet velocity. Similar results were obtained at other directivity angles. Again, additional spectral data for the baseline configuration can be obtained from references 1 to 3 and 5 to 7.

EFFECT OF PERFORATED-SURFACE FLAPS

Perforated Trailing-Edge Flap Surfaces

The initial effort at reducing jet-flap interaction noise was by the use of perforated surfaces near the trailing edge of the second flap. Surface porosities of 44, 15, and 4 percent open area (fig. 7; called configurations 4, 5, and 6) were tested at a jet velocity of 228 meters per second. Typical acoustic results of these tests are given in the following sections.

Overall sound pressure level. - The effect on OASPL of using perforated surfaces near the trailing edge of the second flap is shown in figure 18(a) as a function of directivity angle. Also shown in the figure, for comparison, are the OASPL data obtained with a hard surface. No significant differences in OASPL were observed among the three porosities used. Furthermore, and most importantly, the types of perforated trailing edge tested did not attenuate the noise level below that with hard-wall flap surfaces.

Spectra. - Typical spectra are shown in figure 18(b) for the trailing-edge, perforated-surface flaps just discussed. The SPL values in figure 18(b) are shown as a function of frequency for an 85° directivity angle. Also included, for comparison, is the spectrum for the hard-wall flaps. In general, the spectra for the perforated-surface flaps show little noise attenuation, compared with the hard-wall flap spectrum. With a 4-percent porosity, the perforated-surface flaps appear to yield about 1/2 to 1 decibel less noise in the middle-frequency range of 500 to 5000 hertz than the other configurations. The perforated flap surfaces with a 44-percent porosity, on the other hand, show an increase in SPL above about 10 000 hertz.

Perforated Leading- and Trailing-Edge Flap Surfaces

Because perforating only the trailing edge of the second flap had shown substantially no attenuation of the jet-flap interaction noise (fig. 18), it was decided to perforate additionally all the leading-edge surfaces of both flaps and the trailing edge of the first flap (configuration 13). This could possibly lead to attenuation of the noise caused by the jet flow through the flap slots as well as the flow impingement noise on the surfaces constituting the passages or slots. Except as noted, the following acoustic data were obtained by using a 15-percent porosity for the perforated surfaces.

Overall sound pressure level. - The variation of OASPL with directivity angle with all leading- and trailing-edge regions made of perforated plate (configuration 13) is shown in figure 19(a). The OASPL data for hard-wall surfaces are again included in the figure for comparison. A reduction in OASPL of up to 3 decibels was obtained over much

of the forward quadrant. However, little attenuation (less than 1 dB) was obtained at directivity angles of 85° and 100° .

Spectra. - A typical spectrum obtained with configuration 13 is shown in figure 19(b). In the figure, the SPL data are plotted as a function of frequency for an 85° directivity angle. Also shown, for comparison are the data obtained with the hard-wall baseline configuration. In the frequency range from 400 to 1250 hertz, using the perforated surfaces lowered the SPL values by 2 to 4 decibels below those for the hard-wall surfaces. However, at high frequencies (5000 to 20 000 Hz) the SPL values with the perforated surfaces were somewhat higher (1 to 3 dB) than those obtained with the baseline configuration. At other directivity angles (table III) SPL attenuations of as much as 5 decibels were obtained in the middle-frequency range. However, in all cases the perforated surfaces increased the noise in the high-frequency range (4000 to 20 000 Hz) above the baseline values.

Flap Surface Combinations and Geometry Changes

Several combinations of perforated and hard-wall flap surfaces, other than those already discussed, were also studied briefly. These included perforated leading edges for both flaps (configuration 12); perforated trailing edges for both flaps and for the leading edge of the second flap (configurations 9 and 10); perforated trailing edge of first flap and leading edge of second flap (configurations 7 and 11). In addition, the effects of filling the cavities behind the perforated flap surfaces with Scottfelt foam were determined (configurations 8 and 9).

In general, the preceding combinations of treated surfaces did not change the OASPL values and spectra significantly from those obtained with the baseline and treated configurations discussed in the previous sections. The pertinent data are summarized in tables II and III. When the cavities behind the perforated surfaces were filled with Scottfelt foam, there was no measurable increase in OASPL attenuation or significant spectral change, compared with the data for the empty cavities. These data are also included in tables II and III.

As part of this series of tests, the slot between the first and second flaps was reduced from 5.84 centimeters to 4.3 centimeters by the addition of a 3.8-centimeter extension to the trailing edge of the first flap (configuration 14). This configuration was a more exact duplication of that used in reference 1. The smaller slot size caused a small reduction in SPL ($1\frac{1}{2}$ dB) in the 200- to 800-hertz frequency range compared with that for the standard slot. A reduction of about 1 decibel in OASPL was also obtained except directly under the configuration (directivity angles of 85° to 115°). The data for configuration 14 are included in tables II and III.

The initial wing-flap system had chordwise structural ribs extending through the flap slots to help secure the flaps to the wing. The ribs were located 61 centimeters to each side of the nozzle centerline. In the latter part of the program, these ribs were removed to ascertain their contribution to the jet-flap interaction noise. No measurable contribution to the noise level could be related to the presence of these ribs (tables II and III).

EFFECT OF OFF-THE-SURFACE SCREENS

The largest noise attenuation in the investigation was obtained by using screens to alter the turbulence structure of the jet in the vicinity of the flap surfaces. The screens were used with the hard-wall baseline configuration as well as with configurations having various combinations of perforated surfaces at the leading and trailing edges of the flaps. As described in the section APPARATUS AND PROCEDURE, the screens used consisted of (1) a large screen parallel to the flap surfaces covering the jet impingement area on the flaps; (2) a small ramp screen at the trailing edge of the second flap; and (3) a combination of both the preceding screens. The results of these tests are given in the succeeding sections.

Jet-Flow-Impingement-Area Screens

Overall sound pressure level. - The effect of placing a large screen near the flap surfaces (configurations 19 and 24) on the OASPL of the wing-flap system is shown in figure 20(a). Although configuration 21 had hard-wall flap surfaces, whereas configuration 24 had perforated flap surfaces on the leading and trailing edges of both flaps, the noise attenuation for both configurations was within 1/2 decibel in the forward quadrant. Also shown are the data for the hard-wall baseline configuration. Furthermore, although the screens were also different for the two configurations shown, the acoustic data were substantially the same. In both cases, the OASPL was attenuated at all directivity angles. The maximum noise attenuation in the forward quadrant was 3 decibels (compared with the baseline configuration data). At 85° and 115° , the attenuations were only 1 and 1/2 decibel, respectively. We concluded from this result that the major contributor to the noise reduction was the screen and not the perforated flap surfaces.

Spectra. - Typical spectra for configurations 19 and 24 as well as the hard-wall baseline configuration are shown in figure 20(b). Both screened configurations show reductions in SPL in the middle-frequency range compared with the hard-wall baseline configuration. The perforated-flap configuration (configuration 24) had as much as a 7-decibel reduction (500 Hz). With hard-wall flap surfaces, a noise reduction of only

$3\frac{1}{2}$ decibels was accomplished. At frequencies greater than 2500 hertz, however, large increases in noise (up to 18 dB) were obtained with the screened configurations. The increase in noise at high frequencies was greatest for the screen with the coarser mesh and with the larger screen standoff height from the flap surfaces (configuration 18). This coarse-mesh screen was only 66 centimeters wide, in contrast to the 91.4-centimeter width of the small-mesh screen used with configuration 19. However, the wider screen was placed closer to the flap surface.

Trailing-Edge Ramp Screens

Overall sound pressure level. - The OASPL's for wing-flap systems with a ramp screen at the trailing edge of the second flap are shown in figure 21(a) as a function of directivity angle. Also shown, for comparison, are the OASPL values for the hard-wall flap baseline configuration. As indicated by the data in figure 21(a), the OASPL increased, compared with baseline configuration values, at substantially all directivity angles of interest (10° to 115°) when ramp screens were used. The increase in OASPL amounted to as much as $2\frac{1}{2}$ decibels at an 85° directivity angle with a coarse-mesh (1.2 by 1.2 by 0.157 cm) ramp screen.

Spectra. - Typical SPL data for the preceding configurations are shown in figure 21(b) as a function of frequency. No attenuation was achieved at any frequency compared with the baseline data by using the ramp screen. Sound pressure levels for both ramp screen configurations were above the baseline values at high frequencies. In particular, for configuration 16, which had a coarse-mesh screen and the largest screen standoff height from the flap surfaces, the difference in SPL increased over a wide range of frequencies (500 Hz and higher), reaching a value of 21 decibels above the baseline SPL at 20 000 hertz. From the data of figure 21(b) it is evident that ramp screens at the trailing edge of the second flap can be severe noise generators for EBF-UTW configurations. Also, from the similarity of the high-frequency noise increases with the ramp screen and the large jet-flow-impingement-area screen (figs. 21(b) and 20(b), respectively), this noise appears to be caused by the screening near the flap trailing edge rather than by the large impingement-area screen. This high-frequency noise is primarily a function of the screen standoff height from the flap surfaces (or the projection into the jet flow for the ramp screen).

Combined Screens

Overall sound pressure level. - The effect on OASPL of using a combined screen system, both the jet-flow-impingement-area screen and the ramp screen on the trailing

edge of the second flap, is shown in figure 22(a). Also shown for comparison are the OASPL data for the hard-wall baseline configuration. All the data in figure 22(a) were obtained with 66-centimeter-wide screens with a screen mesh of 1.2 by 1.2 by 0.157 centimeter. Attenuations of as much as 3 decibels with configuration 23 and about 1/2 decibel with configuration 17 were achieved in the forward quadrant. The greater attenuation with configuration 23 is apparently due to its smaller screen standoff height and perforated flap surfaces. Hard-wall flap surfaces and a larger screen standoff height were used with configuration 17.

Spectra. - Typical spectra for the combined ramp- and jet-flow-impingement-area screen configurations are shown in figure 22(b) in terms of SPL as a function of frequency. At frequencies greater than 2500 hertz the SPL values for both screened configurations are greater than those for the baseline hard-wall flap configuration. The high-frequency SPL values are similar in magnitude to those shown in figures 20(b) and 21(b) for each individual screen configuration. The SPL values at frequencies from 50 to 2500 hertz are less, by as much as 7 decibels (500 Hz), with the combined screen configurations than with the baseline configuration. This SPL reduction accounts for the OASPL attenuation noted in the discussion of figure 22(a).

FLAP SURFACE DYNAMIC PRESSURES

As part of this program, a cursory effort was made to determine experimentally the gross relation between dynamic pressures measured on the flap surfaces and the acoustic measurements made in the far field. The dynamic surface pressure spectra in acoustic terms are shown in figure 23 for the second flap of the hard-wall baseline flap configuration (fig. 12). Also shown for comparison is the far-field acoustic spectrum shape for the baseline configuration. In general, the leading-edge dynamic pressure data (3) and those obtained near the flap trailing edge (1) produced similar slopes (3.5 dB/octave) at frequencies above 400 hertz. The dynamic pressure slope at 13 centimeters from the leading-edge transducer (2) was somewhat greater (4.5 dB/octave) than for the other two locations. This greater slope may have been caused by the location of the transducer near the jet flow impact region on the flap. The other transducers were located in the circulation flow region around the flap.

The slopes of the dynamic surface pressure data for transducers 1 and 3 agree fairly well with the slope of the far-field acoustic data above 800 hertz at directivity angles of 85° and 100° . At directivity angles of 40° , 55° , and 70° , however, the far-field acoustic curve shows an increasing change in slope, going from 3 decibels per octave from 800 to 3150 hertz to 6 decibels per octave between 3150 and 20 000 hertz. None of the dynamic pressure data show this change in slope. At a directivity angle of 155° , the best agreement with the far-field curve is the data obtained with transducer 2. For

frequencies less than 200 hertz, the overall slopes of the far-field curves are much greater (5 dB/octave) than those of the data with the transducers (2 dB/octave).

From the similarity of the slopes of the acoustic and dynamic pressure data (directivity angles of 85° and 100° and frequencies greater than 400 Hz), it can be inferred that the far-field noise spectra are related to the surface pressure fluctuations by a relatively simple transfer function. At low frequencies (less than 200 Hz), no such relation is evident. This may indicate that the transfer function is a complex relation involving the flow field and configuration geometry of the particular wing-flap configuration. Further analysis of these data is beyond the scope of this report.

CONCLUDING REMARKS

Several potential means for reducing the jet-flap interaction noise of externally blown flap, under-the-wing configurations have been investigated acoustically. Presentation and discussion of the data generally were limited to a microphone position closest to directly below the aircraft for the approach condition (directivity angle, 85°). While larger jet-flap noise attenuation occurred in the forward quadrant at directivity angles near 55° than directly under the model, these angles are not of great interest in developing aircraft noise footprints. However, they are of interest for studying jet-flap noise mechanisms (which is beyond the scope of this report). For this reason, the noise data in the forward quadrant are included in tables II and III. The major contributor to the noise reduction through the use of a perforated flap surface covered with a large screen was the screen and not the perforated surface.

None of the present efforts to reduce jet-flap interaction noise were effective over the entire frequency range of the spectrum over a nozzle jet velocity range of 166 to 258 meters per second. The effect of velocity on the noise differences was minimal. In nearly all instances, the noise reductions at low- and middle-frequency ranges with the present attenuation devices were accompanied by an increase in high-frequency noise. If the present data were scaled to a full-size aircraft (a factor of a least 4), the consequent frequency shift of the increased high-frequency noise could produce adverse acoustic effects in the most annoying region of the spectrum. In addition, the marginal noise reductions offered by the devices tested herein (maximum reduction of less than 4 dB in overall sound pressure level) would be offset by inherent penalties in weight, structural complexity, and aerodynamic performance.

Lewis Research Center,
National Aeronautics and Space Administration,
Cleveland, Ohio, December 12, 1975,
505-03.

APPENDIX - SYMBOLS

C_p	pressure coefficient, $C_p = (P_l - P_{atm}) / (\rho_l U_l^2 / 2)$
f	frequency, Hz
G_1	outer-span gap between first and second flap, cm
G_2	center-span gap between first and second flap, cm
G_3	gap between wing and flap, cm
P	pressure, N/m^2
U_l	exhaust jet velocity, m/sec
V_N	fully expanded ideal nozzle exhaust velocity (jet velocity), m/sec
X	flap chord coordinate
Y	height of rake tube end above impact surface of flap, cm
Y_1	flap surface coordinate, above chord line
Y_2	flap surface coordinate, below chord line
θ	microphone radial angle measured from nozzle inlet (directivity angle), deg
ρ	density of undisturbed fluid, kg/m^3

Subscripts:

l	local
atm	atmospheric

REFERENCES

1. Clark, B.; Dorsch, R.; and Reshotko, M.: Flap Noise Prediction Method for a Powered Lift System. AIAA Paper 73-1028, Oct. 1973.
2. Dorsch, R. G.: Externally Blown Flap Noise Research. SAE Paper 740468, Apr. - May 1974.
3. Dorsch, R. G.; Goodykoontz, J. H.; and Sargent, N. B.: Effect of Configuration Variation on Externally Blown Flap Noise. AIAA Paper 74-190, Jan. - Feb. 1974.
4. Hayden, Richard E.; Kadman, Yoram; and Chauuald, Robert C.: A Study of the Variable Impedance Surface Concept as a Means for Reducing Noise from Jet Interaction with Developed Lift Augmenting Flaps. (Rept. 2399, Bolt, Beranek, and Newman, Inc., NAS1-9559), NASA CR-112166, 1972.
5. Dorsch, R. G.; Kriem, W. J.; and Olsen, W. A.: Externally-Blown-Flap Noise. AIAA Paper 72-129, Jan. 1972.
6. Dorsch, R. G.; Krejsa, E. A.; and Olsen, W. A.: Blown Flap Noise Research. AIAA Paper 71-745, June 1971.
7. Olsen, William A.; Dorsch, Robert G.; and Miles, Jeffrey H.: Noise Produced by a Small Scale, Externally Blown Flap. NASA TN D-6636, 1972.
8. Hayden, Richard E.: Sound Generation by Turbulent Wall Jet Flow over a Trailing Edge. Purdue University, 1970.

TABLE I. - FLAP CONFIGURATIONS




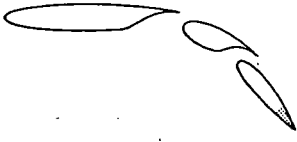

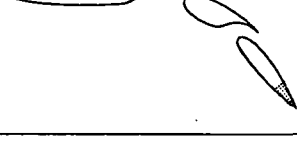
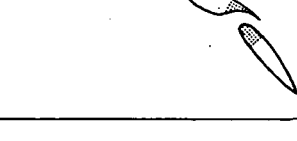

Configuration	Sketch	Description
1		33-Centimeter-diameter conical nozzle
2		Baseline configuration, all flap surfaces solid
3		All flap surfaces solid; two ribs removed, at 61 cm to each side of jet centerline, between first and second flaps
4		Perforated surface on trailing edge of second flap; 44 percent of area open; 0.38-cm-diameter holes spaced 0.56 cm apart and staggered; 0.127-cm skin thickness (fig. 7)
5		Perforated surface on trailing edge of second flap; 4 percent of area open; 6.3-cm-diameter holes spaced 2.54 cm apart and staggered; 0.32-cm skin thickness (fig. 7)
6		Perforated surface on trailing edge of second flap; 15 percent of area open; 0.157-cm-diameter holes spaced 0.4 cm apart and staggered; 0.127-cm skin thickness (fig. 7)
7		Perforated surfaces on trailing edge of first flap and on leading edge of second flap; 44 percent of area open (fig. 7)
8		Perforated surfaces on trailing edge of first flap and on leading edge of second flap; 15 percent of area open; packed with Scottfelt 900 (firmness 3)

TABLE I. - Continued.



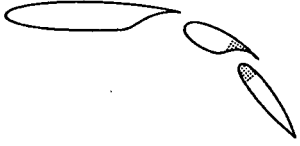



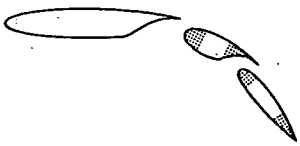
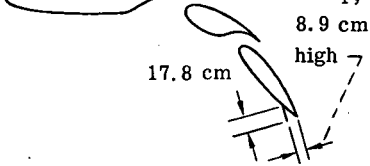
Configuration	Sketch	Description
9		Perforated surfaces on trailing edges of both flaps and on leading edge of second flap; 15 percent of area open; packed with Scottfelt 900 (firmness 3)
10		Perforated surfaces on trailing edges of both flaps and on leading edge of second flap; 15 percent of area open
11		Perforated surfaces on trailing edge of first flap and on leading edge of second flap; 15 percent of area open
12		Perforated surfaces on leading edges of first and second flaps; 15 percent of area open
13		All leading- and trailing-edge surfaces perforated; 15 percent of area open
14		Perforated surfaces on leading edges of both flaps; 15 percent of area open; same gap width as in EBF design of ref. 3
15		Perforated surfaces on all leading and trailing edges; 15 percent of area open; 0.157-cm-diameter holes spaced 0.4 cm apart and staggered; 0.13-cm-skin thickness; two ribs removed, at 61 cm to each side of jet centerline, between first and second flaps
16		All flap surfaces solid; ramp screen (1.2 by 1.2 by 0.157 cm, 66 cm wide, and 63.4-percent open area) on trailing edge of second flap (fig. 8)

TABLE I. - Concluded.

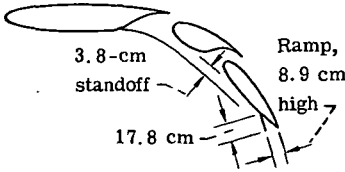
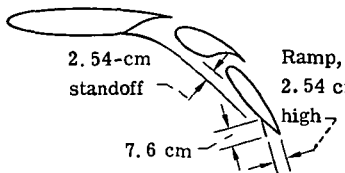
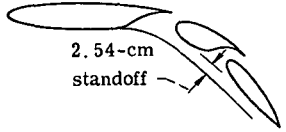
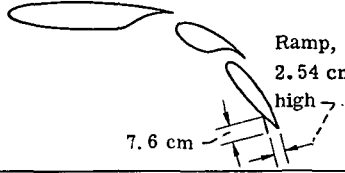
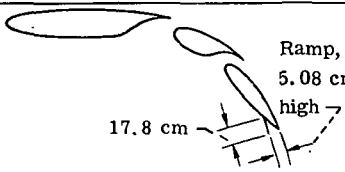
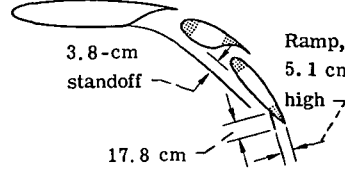
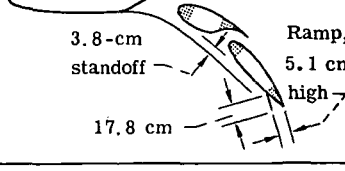
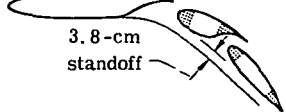
Configuration	Sketch	Description
17	 <p>3.8-cm standoff</p> <p>17.8 cm</p> <p>Ramp, 8.9 cm high</p>	<p>All flap surfaces solid; impingement-area and ramp screens (1.2 by 1.2 by 0.157 cm, 66 cm wide, and 63.4-percent open area); ramp screen on trailing edge of second flap (fig. 8)</p>
18	 <p>2.54-cm standoff</p> <p>7.6 cm</p> <p>Ramp, 2.54 cm high</p>	<p>All flap surfaces solid; impingement-area and ramp screens (2.8 by 2.8 by 0.08 cm, 91.4 cm wide and 39.8-percent open area); ramp screen on trailing edge of second flap; two ribs removed, at 61 cm to each side of jet centerline, between first and second flaps</p>
19	 <p>2.54-cm standoff</p>	<p>All flap surfaces solid; impingement-area screen (2.8 by 2.8 by 0.08 cm, 91.4 cm wide, and 39.8-percent open area); two ribs removed, at 61 cm to each side of jet centerline between first and second flaps (fig. 8)</p>
20	 <p>7.6 cm</p> <p>Ramp, 2.54 cm high</p>	<p>All flap surfaces solid; ramp screen (2.8 by 2.8 by 0.08 cm, 91.4 cm wide, and 39.8-percent open area); two ribs removed at 61 cm to each side of jet centerline, between first and second flaps (fig. 8)</p>
21	 <p>17.8 cm</p> <p>Ramp, 5.08 cm high</p>	<p>All flap surfaces solid; ramp screen (1.2 by 1.2 by 0.157 cm, 66 cm wide, 53.4-percent open area); two ribs removed at 61 cm to each side of jet centerline, between first and second flaps (fig. 8)</p>
22	 <p>3.8-cm standoff</p> <p>17.8 cm</p> <p>Ramp, 5.1 cm high</p>	<p>All leading- and trailing-edge surfaces perforated (15-percent open area); impingement-area and ramp screens (1.2 by 1.2 by 0.157 cm, 66 cm wide, and 63.4-percent open area); ramp screen on trailing edge of second flap (figs. 7 and 8)</p>
23	 <p>3.8-cm standoff</p> <p>17.8 cm</p> <p>Ramp, 5.1 cm high</p>	<p>Same as configuration 22, but with two ribs removed, at 61 cm to each side of jet centerline between first and second flaps</p>
24	 <p>3.8-cm standoff</p>	<p>All leading- and trailing-edge surfaces perforated (15-percent open area); impingement-area screens (1.2 by 1.2 by 0.157 cm, 66 cm wide, and 63-percent open area); two ribs removed, at 61 cm to each side of jet centerline between first and second flaps (fig. 8)</p>

TABLE II. - ATTENUATIONS (+) AND AMPLIFICATIONS (-) IN OVERALL SOUND PRESSURE
LEVEL (OASPL) AT 15.24-METER RADIUS

Configuration	Jet velocity, V_N , m/sec	Directivity angle, θ , deg					Configuration	Jet velocity, V_N , m/sec	Directivity angle, θ , deg				
		10	10-90	90	90-180	180-360			10	10-90	90	90-180	180-360
		Change in OASPL, dB (re 20 μ N/m ²)							Change in OASPL, dB (re 20 μ N/m ²)				
1	166	+25.5	+28	+26.5	+23.5	+14	17	166	0	-0.5	-1	-2	+3
	228	+28	+28	+25.5	+22	+12.5		228	+0.5	+0.5	0	+2	+3
	258	+27	+27	+25.5	+22	+11.5		258	+0.5	+0.5	+1	+2	+2.5
4	166	0	+0.5	+1	+0.5	+1.5	14	166	0	+1.5	+1	+0.5	+0.5
	228	-1	-0.5	0	0	+0.5		228	+0.5	+1.5	+1	+0.5	+0.5
	258	-0.5	0	0	0	+1		258	0	+1	+0.5	0	+1
5	166	0	0	+0.5	+0.5	+2	22	166	+1	+0.5	+0.5	+2	+2.5
	228	-0.5	0	0	0	+1		228	+2	+2.5	+1.5	+2.5	+2.5
	258	-0.5	0	0	0	+1		258	+2	+2.5	+2.5	+3	+3
6	166	+0.5	+0.5	+0.5	0	+1	23	166	+2	+2	+1	+3	+4.5
	228	-0.5	0	-0.5	-0.5	0		228	+2	+2	+1.5	+3	+3
	258	-1	-0.5	-0.5	-0.5	0		258	+2	+2	+2	+2.5	+2.5
7	166	0	+1	0	0	+0.5	15	166	+1	+1.5	0	0	+0.5
	228	0	+0.5	-1	-0.5	0		228	+1.5	+2	0	0	+1
	258	0	-0.5	-1	-1	0		258	+1	+1	0	-0.5	+0.5
8	166	0	+1	+1	-0.5	0	24	166	+1.5	+1	+0.5	+2	+2
	228	+1	+1	0	0	0		228	+2.5	+2.5	+2	+3	+3
	258	0	+1	0	-0.5	0		258	+2	+2	+2	+2.5	+2.5
9	166	0	+1.5	+1	+0.5	+0.5	3	166	-0.5	0	0	0	+0.5
	228	0	+1	-0.5	-0.5	0		228	-0.5	0	0	0	+0.5
	258	0	+1	0	-1	0		258	-0.5	0	-0.5	0	+0.5
10	166	0	+1.5	+0.5	+0.5	+1	18	166	+1	+1.5	+1.5	+1	+3
	228	+1	+1.5	-0.5	-0.5	+0.5		228	+1.5	+2	+2	+2	+3.5
	258	+0.5	+1	-0.5	-1	+0.5		258	+0.5	+1	+1.5	+2	+2.5
11	166	0	+1	+0.5	+0.5	+0.5	19	166	+2	+2	+1.5	+1.5	+3
	228	+1	+1	0	-1	+0.5		228	+2	+2	+1.5	+2.5	+2.5
	258	+1	+1.5	0	-0.5	+1		258	+1	+1.5	+2	+2	+3
12	166	0	+0.5	0	0	0	20	166	-1	-1	-1	-1.5	0
	228	+0.5	+1	0	0	+0.5		228	-1.5	-1	-1	-0.5	-0.5
	258	+1	+1	0	-0.5	+0.5		258	-1	-1	0	0	0
13	166	+1	+2	+1	+1	+1	21	166	-1	-2.5	-2	-1.5	0
	228	+1.5	+2	0	0	+1		228	-1	-1	-1.5	0	0
	258	+1	+1.5	0	+0.5	+1		258	-1.5	-1.5	-0.5	0	0
16	166	-1.5	-1.5	-2	-0.5	+1	17	166	0	-0.5	-1	-2	+3
	228	-1	-1.5	-1.5	0	+0.5		228	+0.5	+0.5	0	+2	+3
	258	-1.5	-1.5	-1	0	0		258	+0.5	+0.5	+1	+2	+2.5

TABLE III. - ATTENUATIONS (+) AND AMPLIFICATIONS (-) IN SOUND PRESSURE LEVEL (SPL) AT 15.24-METER RADIUS

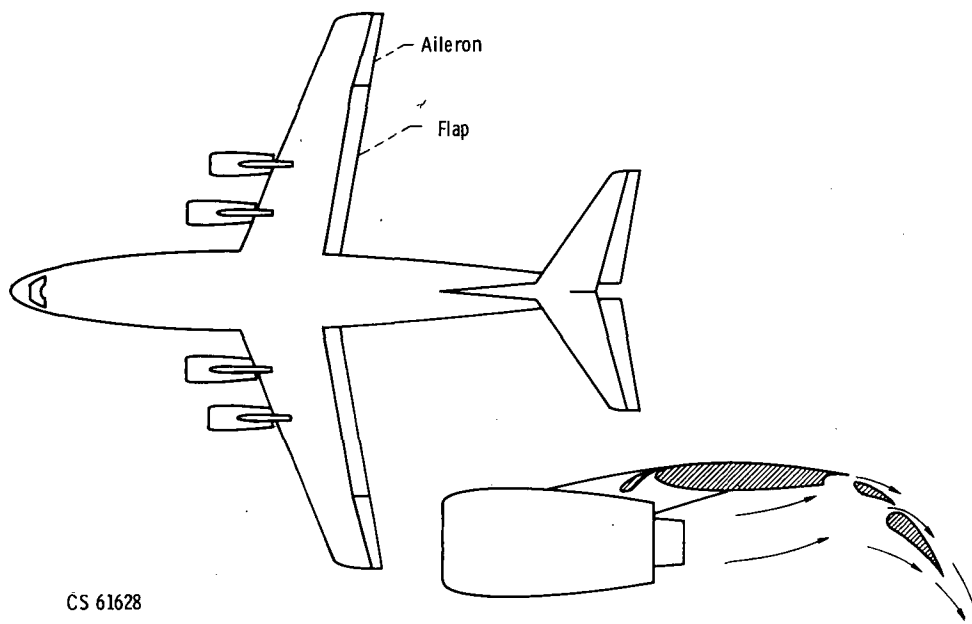
Config-uration	Jet velocity, V_N , m/sec	Direc-tivity angle, θ , deg	Frequency range, Hz				Config-uration	Jet velocity, V_N , m/sec	Direc-tivity angle, θ , deg	Frequency range, Hz			
			50-200	250-800	1000-3150	4000-20 000				50-200	250-800	1000-3150	4000-20 000
			Change in SPL, dB (re 20 $\mu\text{N}/\text{m}^2$)							Change in SPL, dB (re 20 $\mu\text{N}/\text{m}^2$)			
1	166	230	+15	+12	+11	+1.5	11	166	155	+1.5	+2	+2	-5
	228	230	+13	+10	+10	+4		228	155	+2	+1	+1	-3.5
	258	230	+10.5	+8.5	+8.5	+5		258	155	+1	0	+1.5	-2.5
4	166	230	+3	+0.5	0	-8.5	11	166	230	-1	+1	+3	-4.5
	228	230	0	0	+5	-3.5		228	230	-5	-5	+3.5	-5
	258	230	0	+5	0	-1.5		258	230	-5	-1	+2.5	-1.5
5	166	230	+0.5	+1	+1	-1	12	166	40	+1.5	+2	+2.5	-4
	228	230	+5	+5	+1	-5		228	40	+1.5	+1.5	+2.5	-5
	258	230	0	+5	0	-5		258	40	+2	+1.5	+2.5	0
6	166	230	+0.5	0	0	-4	12	166	55	+1	+1.5	+1.5	-4
	228	230	0	0	-5	-3		228	55	+2	+2	+2.5	-1.5
	258	230	0	0	-1	-2		258	55	+2.5	+1.5	+3	0
7	166	230	-1	+0.5	+2.5	-10	12	166	70	+0.5	0	+1.5	-5
	228	230	-1.5	-1	+3	-4.5		228	70	+2	+1.5	+2	-2
	258	230	-1	-2	+2.5	-2		258	70	+2	+5	+2.5	-1
8	166	230	-1	+1	+3.5	-2.5	12	166	100	0	+0.5	-2	-3
	228	230	-5	-1	+2.5	+1		228	100	+5	-5	-1.5	-5
	258	230	-5	-1.5	+3	+2		258	100	+5	-5	-1	0
9	166	230	-1	+0.5	+3	-3.5	12	166	155	+1.5	+2	+2	-5.5
	228	230	-1.5	-1	+3.5	0		228	155	+2	+1	+1	-3.5
	258	230	-1	-2	+3	+2		258	155	+1.5	+5	+5	-2.5
10	166	230	-0.5	+1.5	+3.5	-5	12	166	230	0	0	+2	-3.5
	228	230	-5	0	+3.5	-5		228	230	-5	-1	+3	0
	258	230	-1	-1	+2.5	+1		258	230	0	-1.5	+2	+1
11	166	40	+2.5	+3.5	+4	-4	13	166	40	+2	+3.5	+4.5	-4.5
	228	40	+1.5	+2	+3	-5		228	40	+2	+3	+3.5	0
	258	40	2	+2	+3	0		258	40	+3	+2.5	+4.5	-4
11	166	55	+1.5	+4	+3.5	-4	13	166	55	+1.5	+5	+4	-4
	228	55	+2	+2.5	+3.5	-1		228	55	+2	+3	+4	-1
	258	55	+2	+2.5	+3.5	0		258	55	+2	+3	+3.5	0
11	166	70	+1	+2	+2	-4	13	166	70	+1.5	+2.5	+3	-5
	228	70	+1.5	+2.5	+2.5	-2		228	70	+2.5	+3	+4	-1.5
	258	70	+1.5	+3	+2.5	-1		258	70	+2	+3.5	+3	-1
11	166	100	-0.5	+1	-2	-2.5	13	166	100	-0.5	+1	-3	-2.5
	228	100	0	0	-1.5	0		228	100	+5	-5	-2	-5
	258	100	+1	-1	-1.5	0		258	100	+1	-1	-2	+5

TABLE III. - Continued.

Config-uration	Jet velocity, V_N , m/sec	Direc-tivity angle, θ , deg	Frequency range, Hz				Config-uration	Jet velocity, V_N , m/sec	Direc-tivity angle, θ , deg	Frequency range, Hz			
			50-200	250-800	1000-3150	4000-20 000				50-200	250-800	1000-3150	4000-20 000
			Change in SPL, dB (re 20 $\mu\text{N}/\text{m}^2$)							Change in SPL, dB (re 20 $\mu\text{N}/\text{m}^2$)			
13	166	155	+2	+3	+2.5	-5	22	166	70	+4	+6	+1.5	-18.5
	228	155	+2	+1	+2	-3		228	70	+4	+6	+3	-12.5
	258	155	+1	0	+1	-2		258	70	+4	+6	+3	-9
13	166	230	0	+1	+4	-4	22	166	100	+2	+3	-1.5	-13.5
	228	230	0	0	+4	0		228	100	+3	+4	+1	-6
	258	230	0	-1	+3	+1.5		258	100	+3.5	+4.5	+3.5	-5
16	166	230	0	+0.5	0	-6.5	22	166	155	+3	+6.5	+4.5	-13.5
	228	230	-0.5	+0.5	+0.5	-4		228	155	+3	+5.5	+5	-7
	258	230	0	0	-0.5	-3.5		258	155	+3	+5	+6	-3.5
17	166	40	+3.5	+3	+1	-19.5	22	166	230	+2.5	+5	+7.5	-10
	228	40	+2.5	+3	+1.5	-13.5		228	230	+2.5	+3	+9	-3
	258	40	+2.5	+2.5	+1	-10.5		258	230	+2	+1.5	+7.5	0
17	166	55	+3	+2.5	0	-19	23	166	40	+5	+9.5	+5	-17.5
	228	55	+2.5	+3.5	+1.5	-12		228	40	+5	+6.5	+4.5	-11
	258	55	+2	+2.5	+1.5	-9.5		258	40	+5	+4.5	+3	-10
17	166	70	+2	+0.5	-1.5	-19.5	23	166	55	+5.5	+9.5	+4.5	-17
	228	70	+2	+2.5	+1	-10		228	55	+5	+6.5	+5	-11.5
	258	70	+2	+3	+0.5	-10		258	55	+4	+5	+4.5	-8.5
17	166	100	+1	+1	-2	-14	23	166	70	+4.5	+7.5	+3	-17
	228	100	+2	+2	+0.5	-9		228	70	+5	+6	+4.5	-11
	258	100	+3	+2.5	+1	-6		258	70	+3.5	+5.5	+4	-8.5
17	166	155	+3	+3	+2	-12	23	166	100	+3	+5.5	+1	-12
	228	155	+2	+5.5	+3	-6		228	100	+3	+4	+2.5	-7
	258	155	0	+3.5	+2.5	-6		258	100	+2.5	+4	+3	-5
17	166	230	+6	+4.5	+4	-7	23	166	155	+5	+8.5	+6	-12
	228	230	+2.5	+3	+5	-1.5		228	155	+3	+6	+5	-7.5
	258	230	+1	+2	+4	-1		258	155	+2.5	+5	+5	-4.5
14	166	230	0	0	+2.5	-4	23	166	230	+3.5	+8	+9.5	-8.5
	228	230	+0.5	0	+3.5	0		228	230	+2.5	+3	+9	-2
	258	230	+0.5	-1	+2.5	+1		258	230	+2	+1	+7.5	0
22	166	40	+5	+8	+4	-18.5	15	166	40	+2	+3.5	+3.5	-4.5
	228	40	+5	+6.5	+4	-11		228	40	+1.5	+3.5	+4	0
	258	40	+4	+5.5	+3.5	-9		258	40	+2.5	+2	+2	0
22	166	55	+4.5	+8	+3.5	-18.5	15	166	55	+2	+4	+3.5	-8.5
	228	55	+4	+6.5	+4	-11.5		228	55	+2.5	+3	+4	-0.5
	258	55	+5.5	+5.5	+3	-18.5		258	55	+2	+2	+3	0

TABLE III. - Concluded.

Config-uration	Jet velocity, V_N , m/sec	Direc-tivity angle, θ , deg	Frequency range, Hz				Config-uration	Jet velocity, V_N , m/sec	Direc-tivity angle, θ , deg	Frequency range, Hz			
			50-200	250-800	1000-3150	4000-20 000				50-200	250-800	1000-3150	4000-20 000
			Change in SPL, dB (re 20 $\mu\text{N}/\text{m}^2$)							Change in SPL, dB (re 20 $\mu\text{N}/\text{m}^2$)			
15	166	70	+1	+2	+2.5	-5	18	166	70	+2	+1.5	-1.5	-13
	228	70	+2.5	+3	+3	-1		228	70	+2	+4	+2.5	-6
	258	70	+1.5	+3	+3	-1		258	70	+1	+4	+2	-4
15	166	100	+1	0	-2	-2.5	18	166	100	+1.5	+3	-2	-8
	228	100	0	- .5	- .5	0		228	100	+1.75	+3	+2	-3.5
	258	100	0	-1.5	0	0		258	100	+2	+3	+1.5	-3
15	166	155	+1.5	+2.5	+1.5	-6	18	166	155	+1.5	+3	+1.5	-4
	228	155	+2	+1	+1	-4		228	155	+2	+3	+2.5	-4.5
	258	155	+1	0	+1	-2.5		258	155	+1	+3	+3.5	-1.5
15	166	230	0	+1	+3.5	-4.5	18	166	230	+1.5	+2	+4.5	-1.5
	228	230	0	0	+3.5	+ .5		228	230	+1.5	+2	+5	+3
	258	230	0	-1	+2.5	+1.5		258	230	+ .5	+1	+4.5	+4
24	166	40	+4	+7	+3	-17	19	166	40	+4.5	+5	+1	-13
	228	40	+4	+6.5	+4.5	-10		228	40	+2	+4	+2.5	-6
	258	40	+4.5	+4.5	+3	-9		258	40	+2	+2.5	+1.5	-5
24	166	55	+4	+7.5	+2.5	-18	19	166	55	+3	+4.5	+1	-12
	228	55	+4.5	+6	+5	-9		228	55	+2	+4	+1.5	-6.5
	258	55	+5	+4	+4	-8		258	55	+1.5	+3	+2.5	-4.5
24	166	70	+3	+4.5	+1.5	-16.5	19	166	70	+3	+2.5	-0.5	-11.5
	228	70	+5	+6.5	+4.5	-10		228	70	+1.5	+3.5	+2	-5.5
	258	70	+3.5	+5	+4	-8		258	70	+2	+3.5	+2	-4
24	166	100	+1.5	+4	+1.5	-12.5	19	166	100	+1.5	+3	-2	-7.5
	228	100	+2.5	+4	+1	-7		228	100	+1.5	+3	+1	-3.5
	258	100	+2	+3	+1.5	-4		258	100	+1.5	+2.5	+1.5	-2
24	166	155	+3	+6	+4.5	-10	19	166	155	+2.5	+4	+2.5	-7.5
	228	155	+3.5	+5.5	+5.5	-4.5		228	155	+2	+4	+4	-1.5
	258	155	+2	+4	+5	-2		258	155	+1	+3	+4.5	-1.5
24	166	230	+2	+4	+7	-7	19	166	230	+2	+3.5	+4.5	-1.5
	228	230	+2.5	+3	+8.5	0		228	230	+2	+2.5	+6	+3
	258	230	+2	+1.5	+7	+2.5		258	230	+ .5	+1.5	+5.5	+4.5
3	166	230	-1	-1	-0.5	-3.5	20	166	230	-0.5	-2	-1	-2
	228	230	- .5	0	0	-3.5		228	230	- .5	-1	-1	-1
	258	230	+ .5	-1	- .5	-2.5		258	230	-1	-1.5	-1	-2
18	166	40	+2	+3.5	+1	-13.5	21	166	230	0	0	-0.5	-5.5
	228	40	+1.5	+3.5	+2	-7		228	230	0	- .5	0	-4
	258	40	+1.5	+2.5	-1	-6		258	230	-1	0	-1	-4
18	166	55	+2	+3	+0.5	-13							
	228	55	+2.5	+3.5	+2.5	-6.5							
	258	55	+1.5	+2.5	+2	-5.5							



CS 61628

Figure 1. - Externally blown flap, under-the-wing STOL airplane concept.

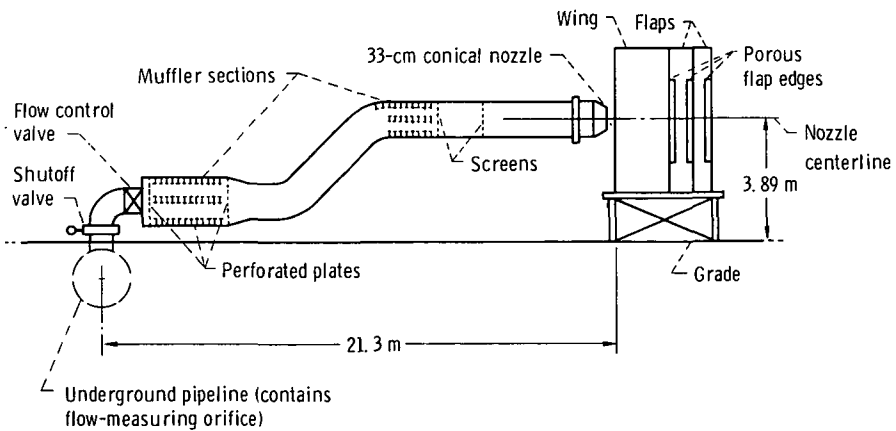


Figure 2. - Test facility with externally blown flap, under-the-wing model on stand.

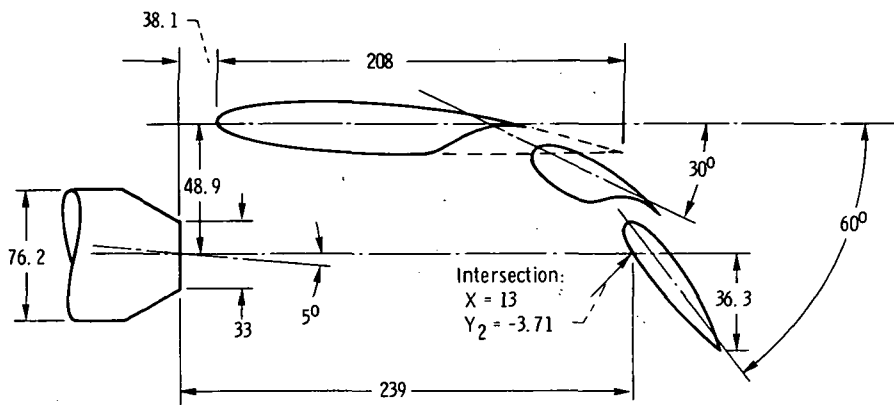
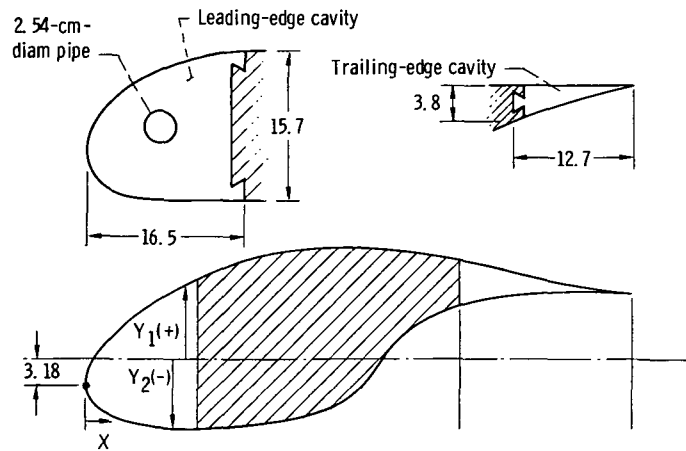
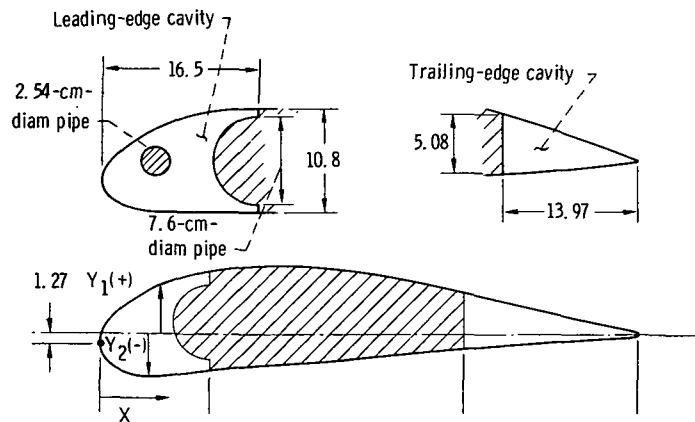


Figure 3. - Nozzle-flap landing configuration. (All dimensions are in cm.)



X	Y ₁	Y ₂	X	Y ₁	Y ₂
0	0	-3.18	31.8	+10.80	0
3.18	+2.96	-6.6	34.9	+10.54	+3.43
6.35	+5.46	-6.99	38.1	+10.16	+5.08
9.53	+7.24	-6.86	41.28	+9.91	+5.97
12.7	+8.51	-6.6	44.45	+9.53	+5.72
15.88	+9.53	-6.35	47.63	+8.89	+6.99
19.05	+10.16	-5.97	50.8	+8.38	+5.72
22.23	+10.54	-5.72	53.98	+5.72	+6.73
25.4	+10.62	-5.08	57.15	+6.73	+6.73
28.58	+10.67	-3.56			

(a) First flap.



X	Y ₁	Y ₂	X	Y ₁	Y ₂
0	0	-1.27	31.8	+5.84	-2.29
3.18	+3.43	-4.19	34.9	+5.88	-1.91
6.35	+5.08	-4.45	38.1	+4.45	-1.65
9.53	+5.97	-4.06	41.28	+3.56	-1.40
12.7	+6.35	-3.81	44.45	+2.92	-1.27
15.88	+6.99	-3.56	47.63	+1.91	-.89
19.05	+7.1	-3.3	50.8	+1.27	-.64
22.23	+6.99	-3.18	53.98	+.64	-.38
25.4	+6.73	-2.79	55.88	+.25	-.127
28.58	+6.35	-2.54			

(b) Second flap.

Figure 4. - Flap cross sections and coordinates. Cavity span width, 14.6 centimeters. (All dimensions are in cm.)

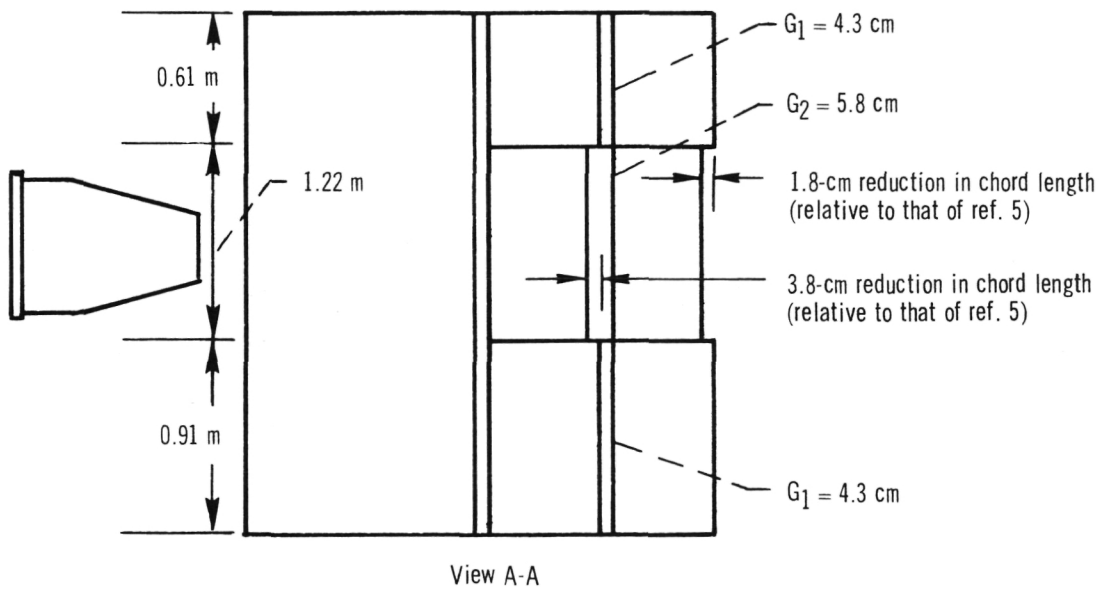
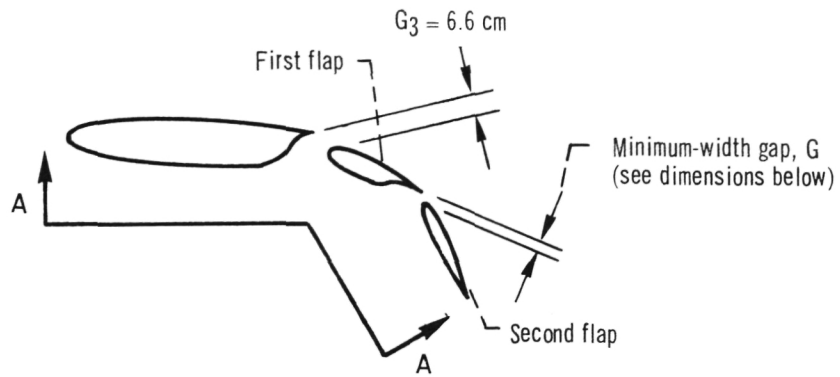


Figure 5. - Baseline hard-wall configuration.

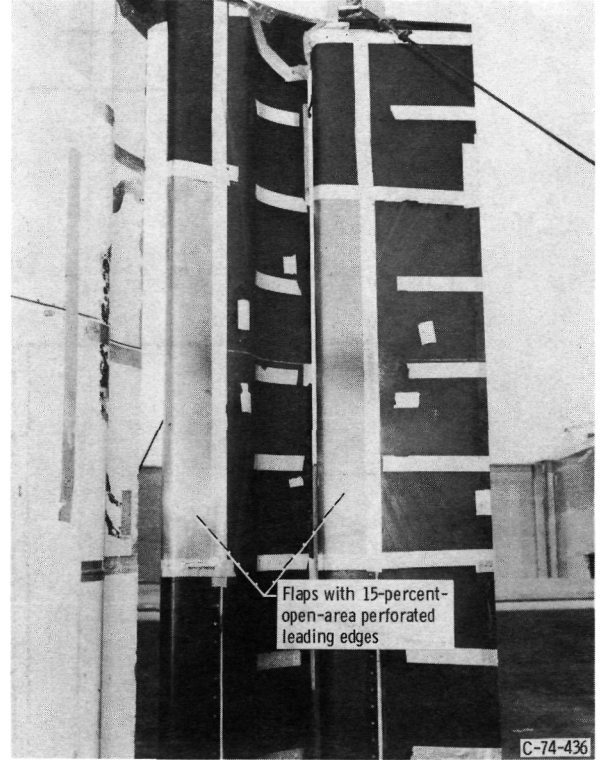
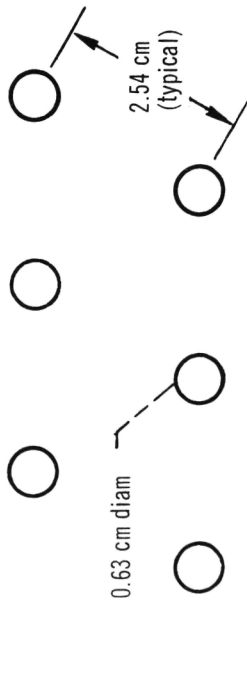
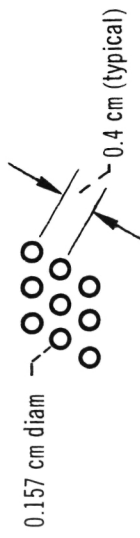


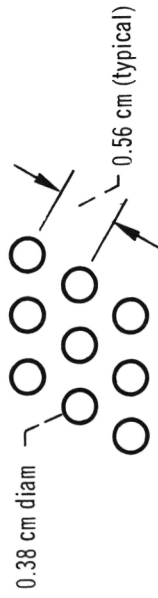
Figure 6. - Representative treated-flap configurations.



(a) 4-Percent open area; 0.32-centimeter sheet aluminum.

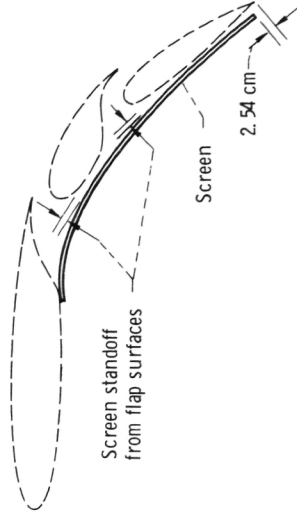


(b) 15-Percent open area; 18-gage (0.13-cm) 304 stainless steel.

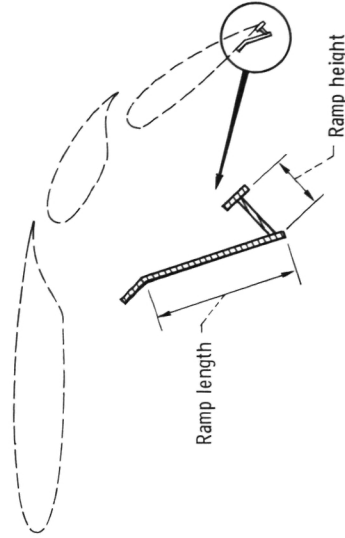


(c) 44-Percent open area; 18-gage (0.13-cm) 304 stainless steel.

Figure 7. - Plan view of flap perforated-surface geometries.



(a) Jet-flow-impingement-area screen.



(b) Trailing-edge ramp screen.

Figure 8. - Screened-flap configurations. (See table I for detailed dimensions.)

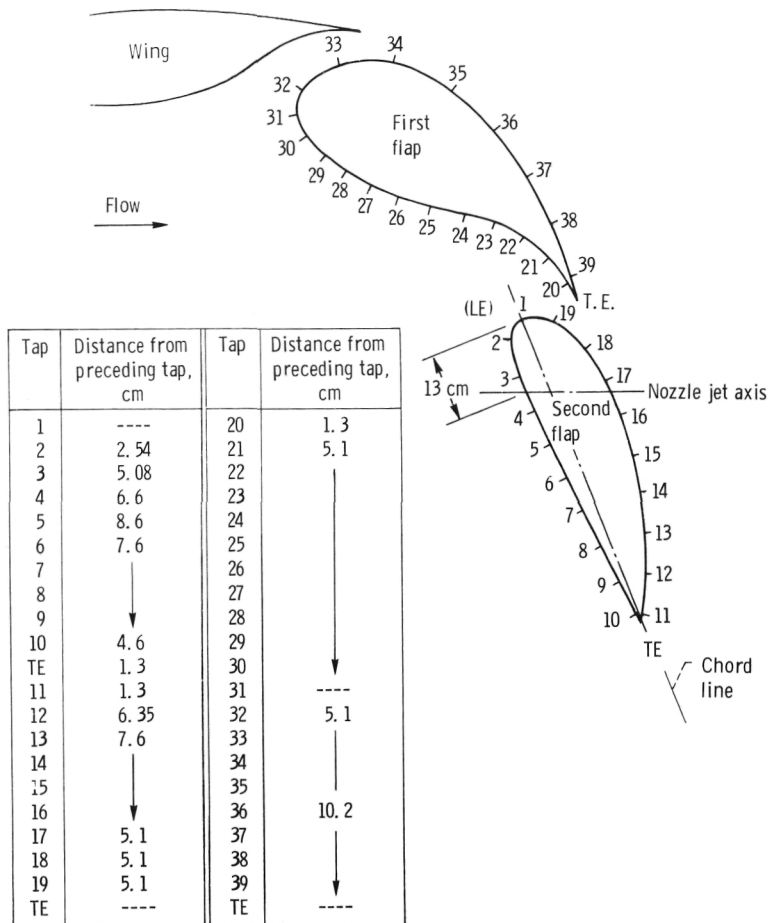


Figure 9. - Static pressure tap locations on flaps.

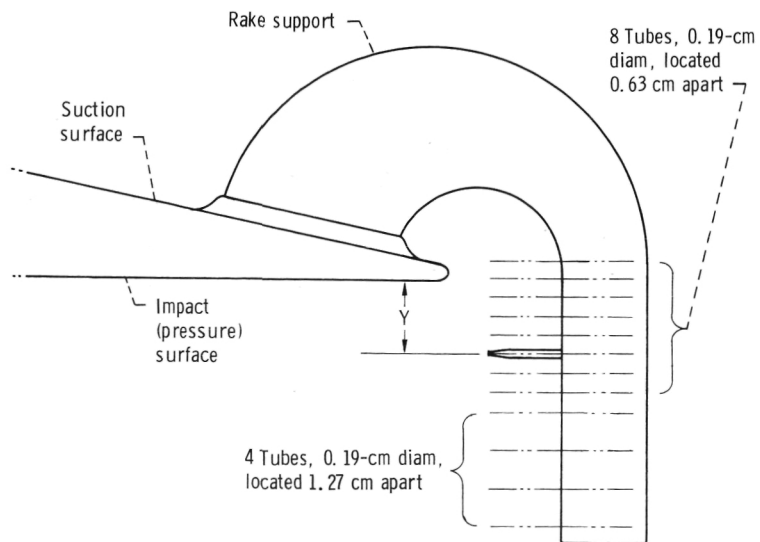


Figure 10. - Twelve-tube, trailing-edge, boundary layer survey rake (located on second flap).

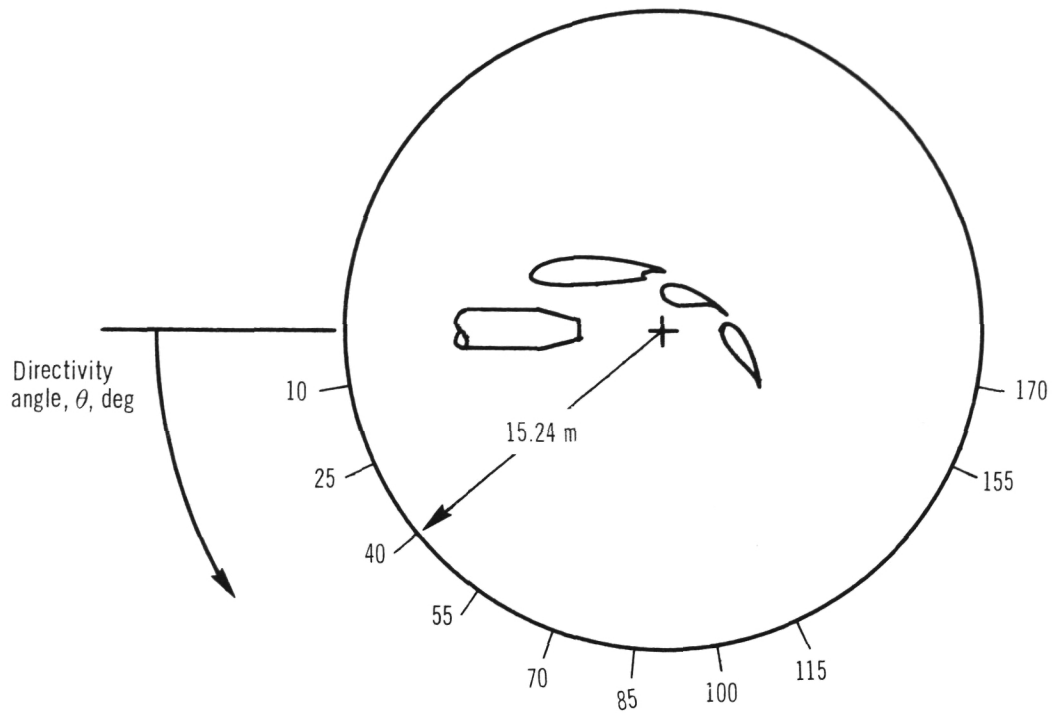


Figure 11. - Microphone locations relative to wing and nozzle.

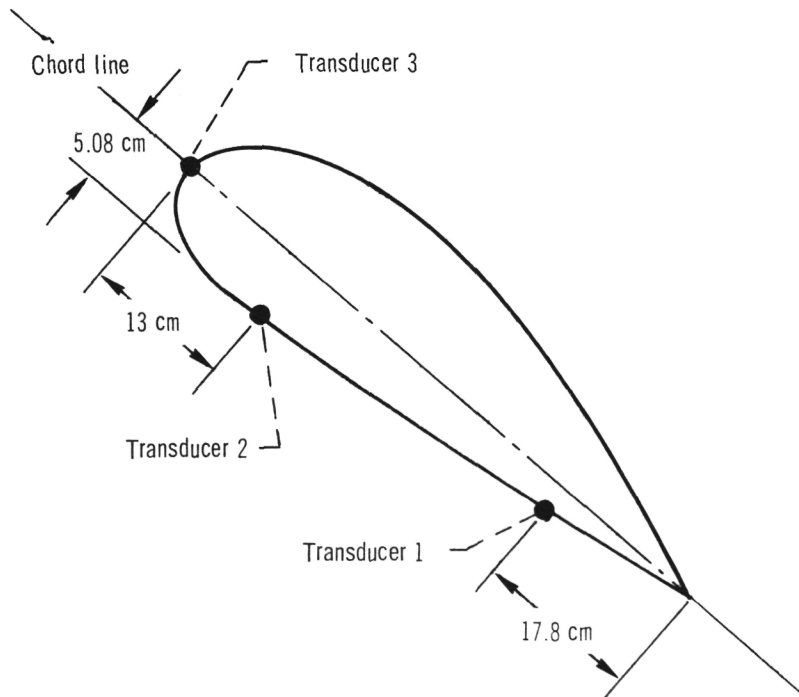
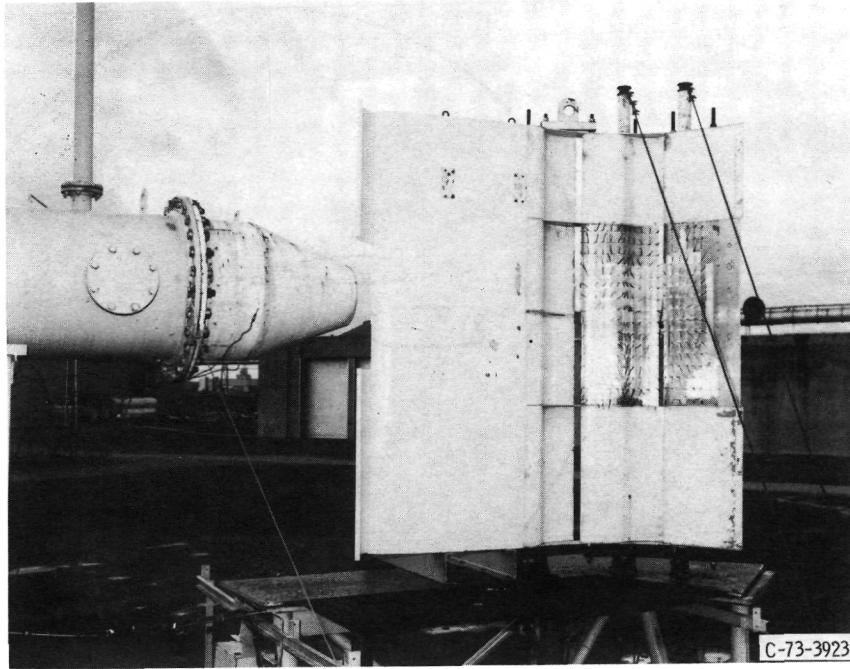
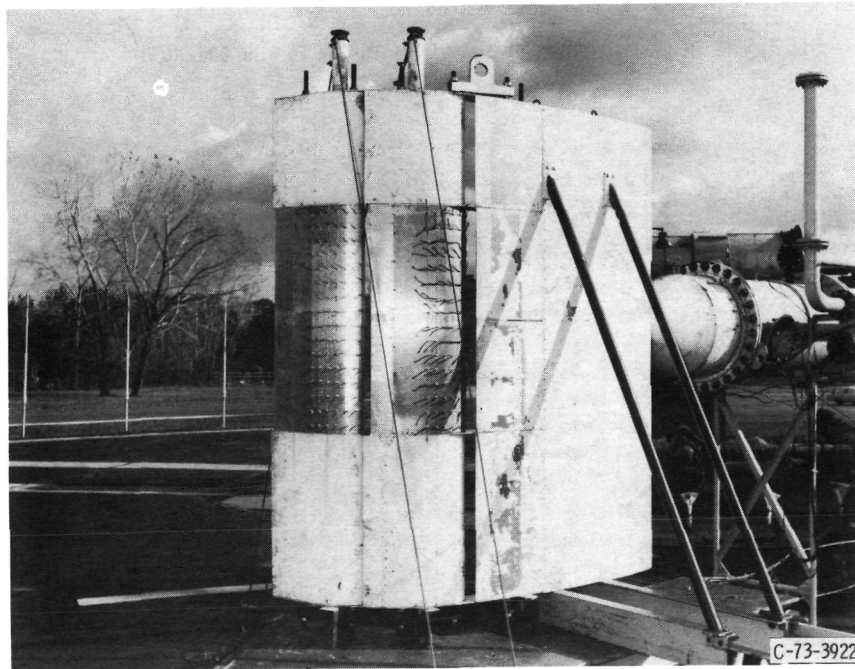


Figure 12. - Transducer locations on second flap.



(a) Lower surfaces.



(b) Upper surfaces.

Figure 13. - Typical flow patterns over externally blown flap, under-the-wing baseline configuration, shown by tufts. Jet velocity, 228 meters per second.

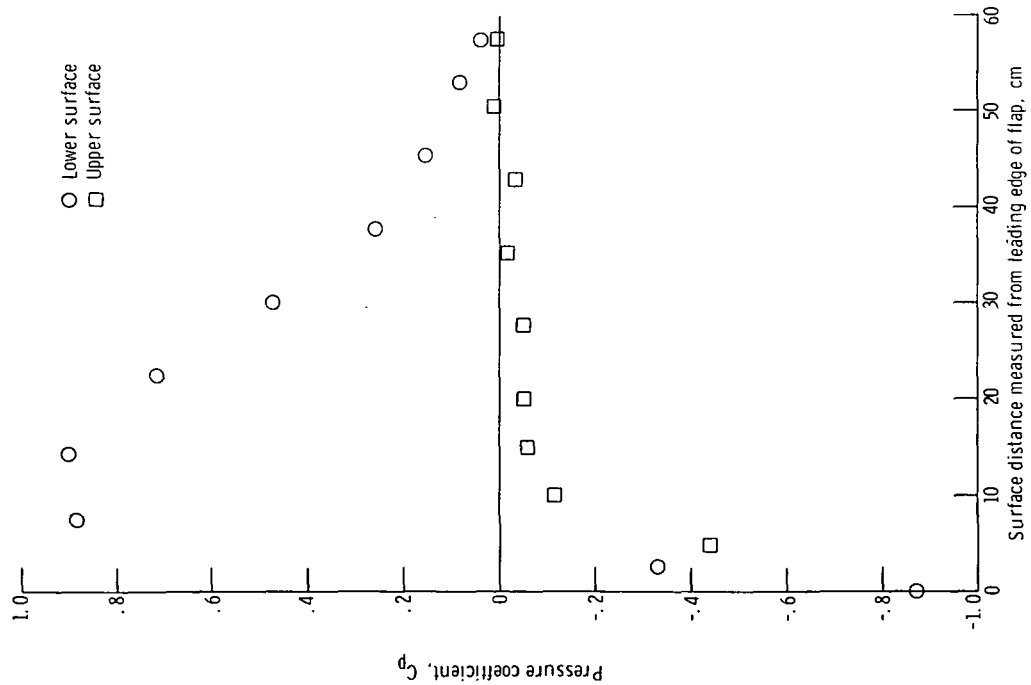


Figure 14. - Pressure distribution over second flap of baseline configuration. Jet velocity, V_N , 228 meters per second.

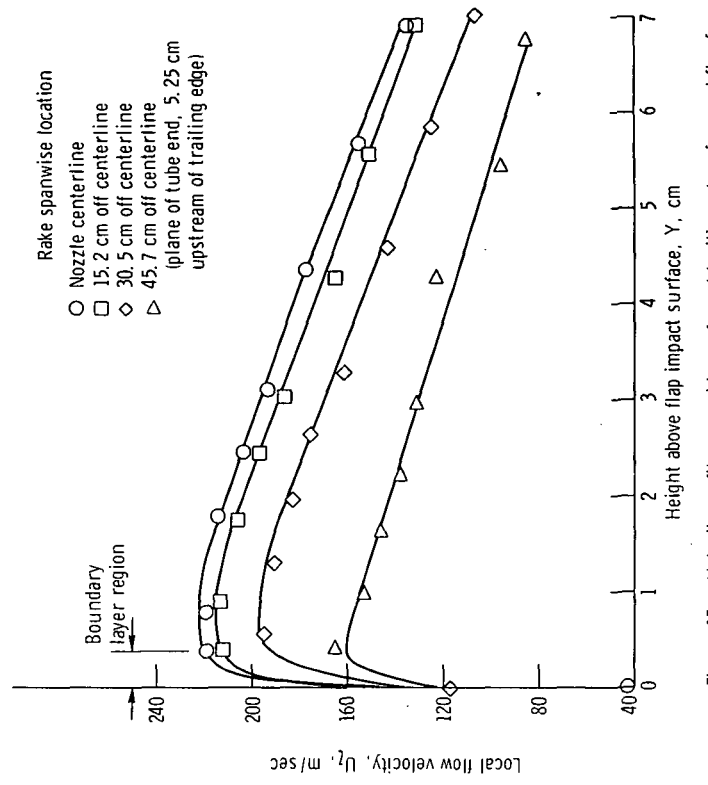


Figure 15. - Velocity profile normal to surface at trailing edge of second flap for baseline flap configuration. Jet velocity, V_N , 228 meters per second.

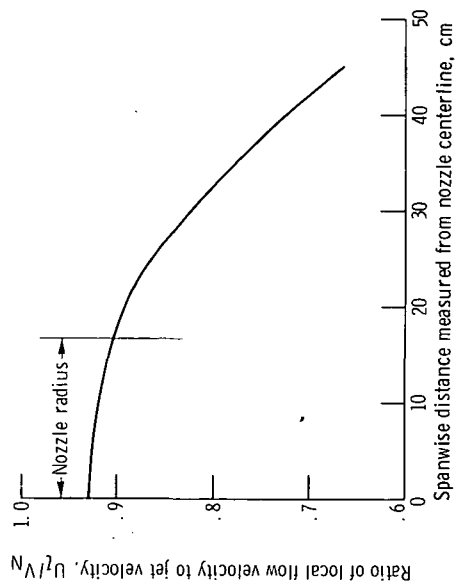
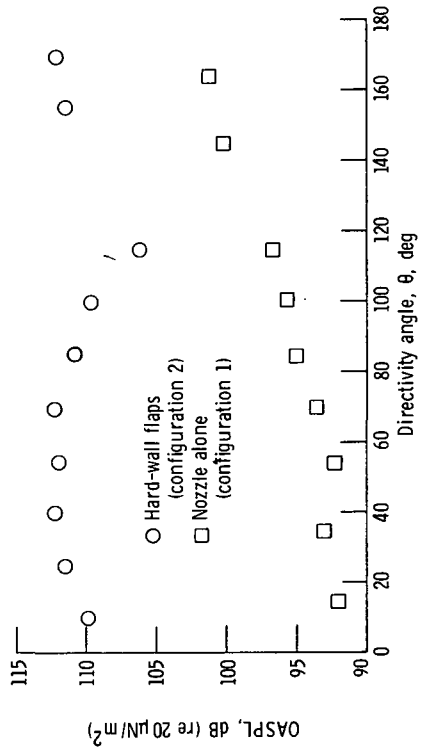
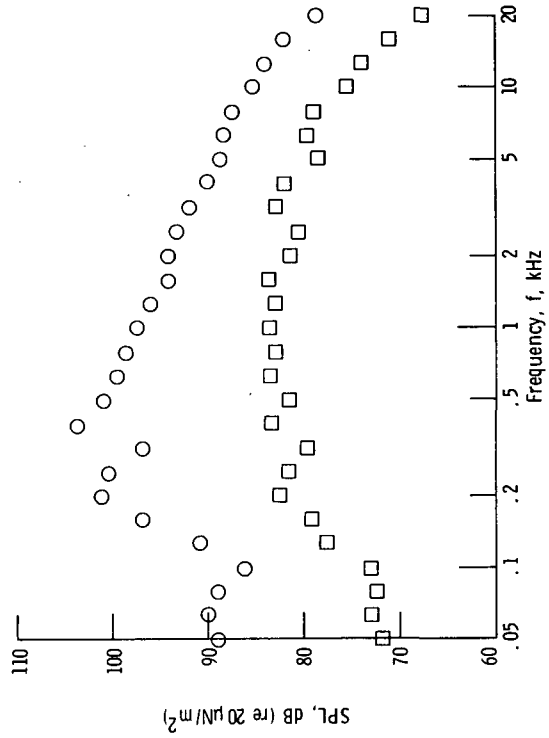


Figure 16. - Spanwise velocity profile at trailing edge of second flap. Height above flap impact surface, Y , 1.1 centimeters; jet velocity, V_N , 228 meters per second.

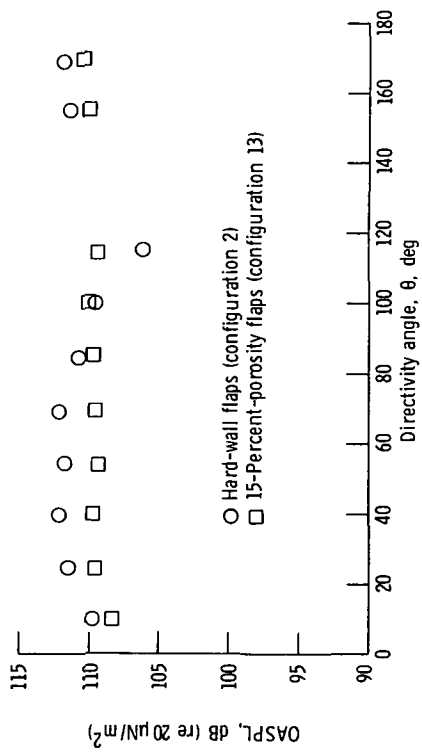


(a) Variation of overall sound pressure level (OASPL) with directivity angle.

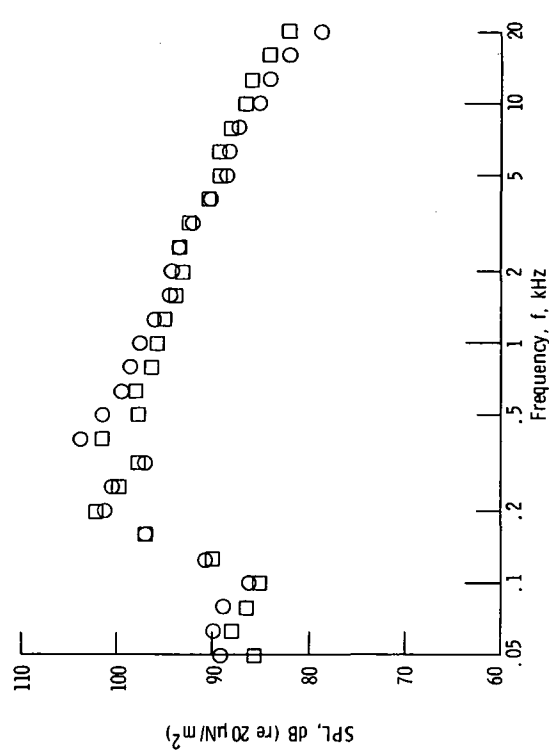


(b) Typical sound pressure level (SPL) spectra. Directivity angle, θ , 85°.

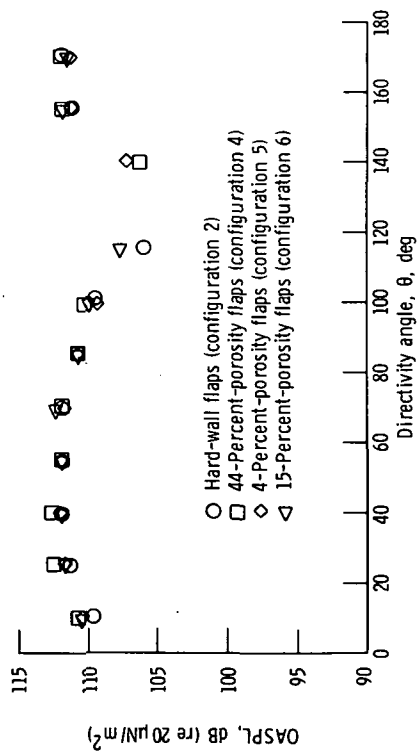
Figure 17. - Typical acoustic characteristics of baseline configuration. Jet velocity, V_N , 228 meters per second.



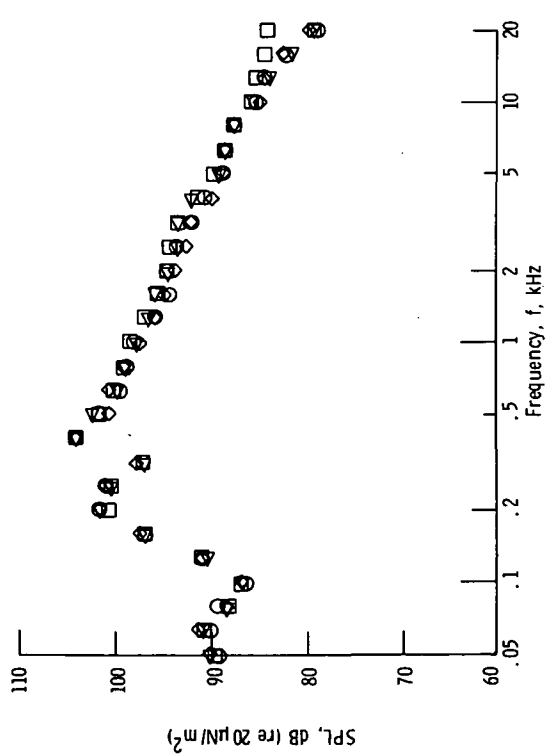
(a) Variation of overall sound pressure level (OASPL) with directivity angle.



(b) Typical sound pressure level (SPL) spectra. Directivity angle, θ , 85°.



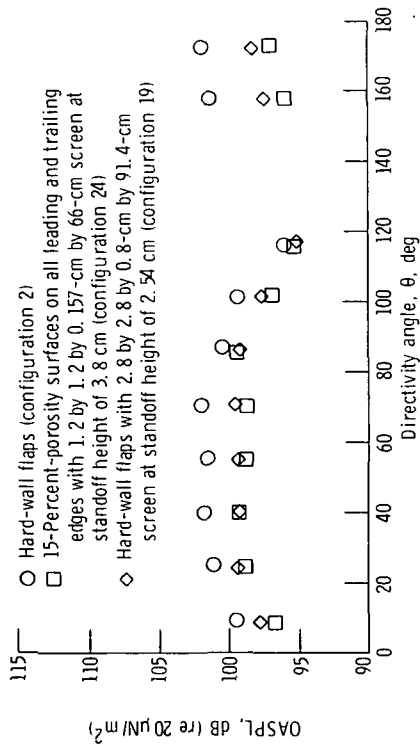
(a) Variation of overall sound pressure level (OASPL) with directivity angle.



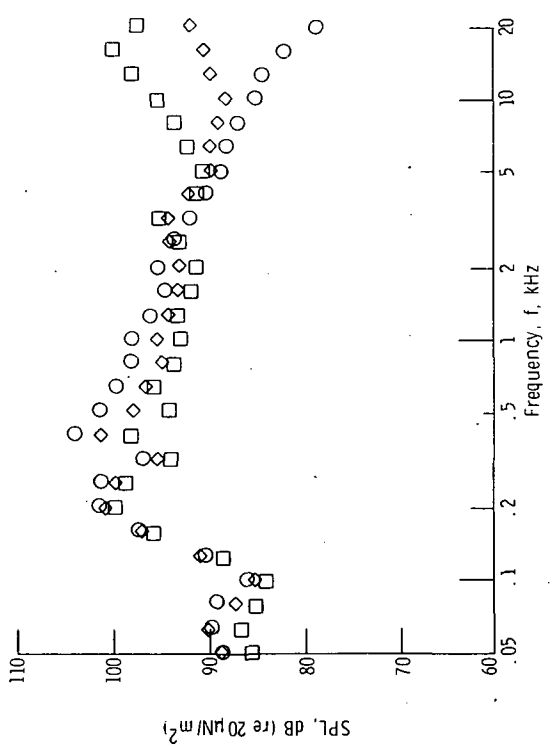
(b) Typical sound pressure level (SPL) spectra. Directivity angle, θ , 85°.

Figure 19. - Typical acoustic characteristics of externally blown flap, under-the-wing configuration with leading- and trailing-edge perforated flap surfaces. Jet velocity, V_N , 228 meters per second.

Figure 18. - Typical acoustic characteristics of externally blown flap, under-the-wing configurations with perforated surfaces near trailing edge of second flap. Jet velocity, V_N , 228 meters per second.

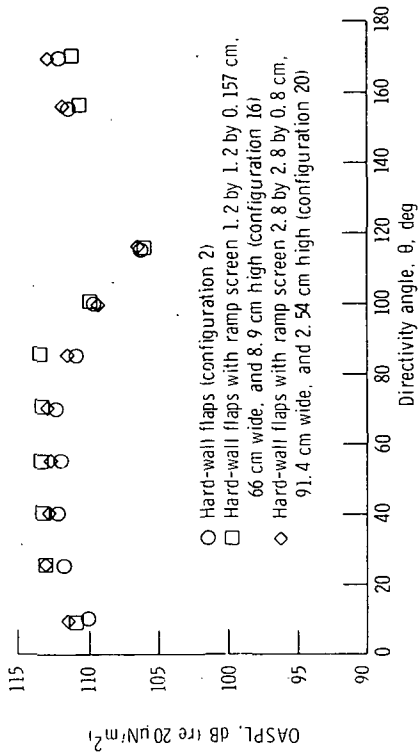


(a) Variation of overall sound pressure level (OASPL) with directivity angle.

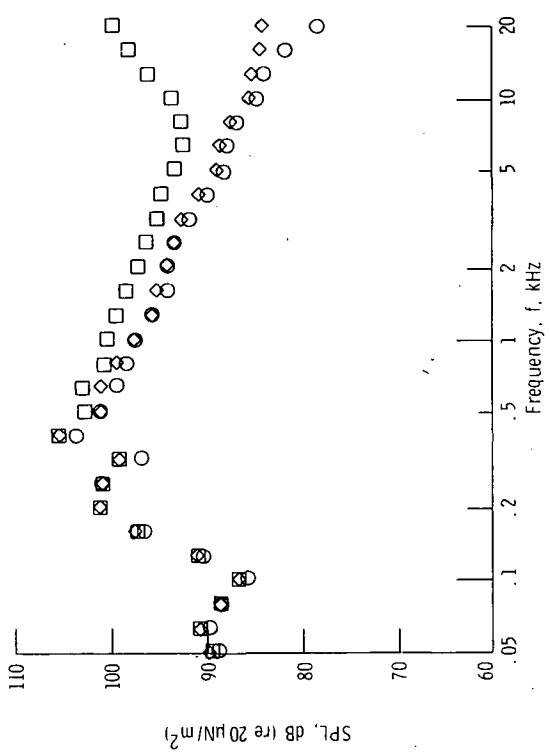


(b) Typical sound pressure level (SPL) spectra. Directivity angle, θ, 85°.

Figure 20. - Typical acoustic characteristics of externally blown flap, under-the-wing configurations with large screen covering jet flow impingement area. Jet velocity, V_N , 228 meters per second.

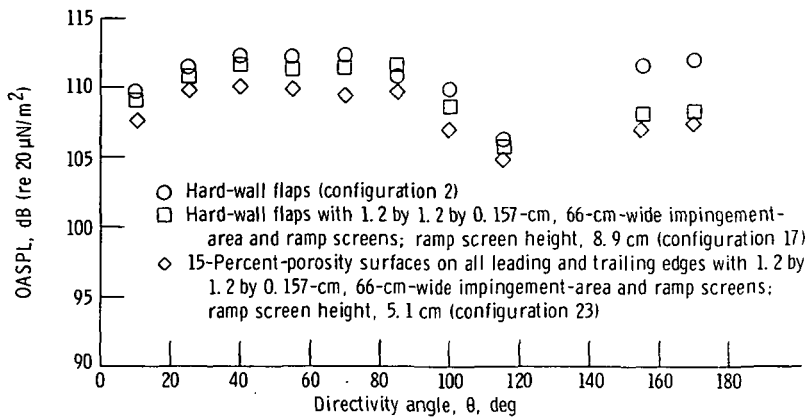


(a) Variation of overall sound pressure level (OASPL) with directivity angle.

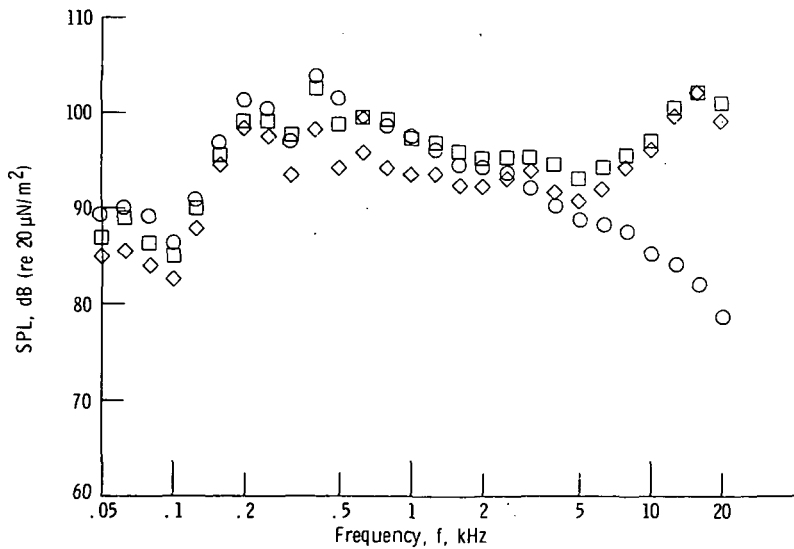


(b) Typical sound pressure level (SPL) spectra. Directivity angle, θ, 85°.

Figure 21. - Typical acoustic characteristics of externally blown flap, under-the-wing configurations with ramp screens at trailing edge of second flap. Jet velocity, V_N , 228 meters per second.

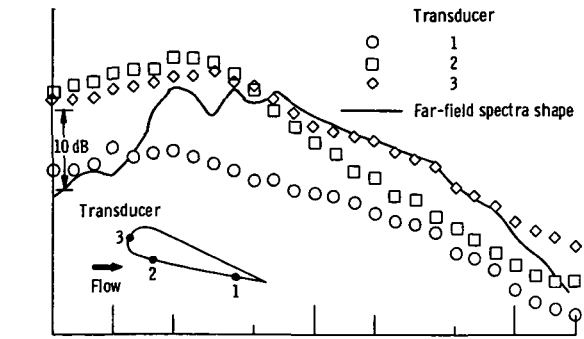


(a) Variation of overall sound pressure level (OASPL) with directivity angle.

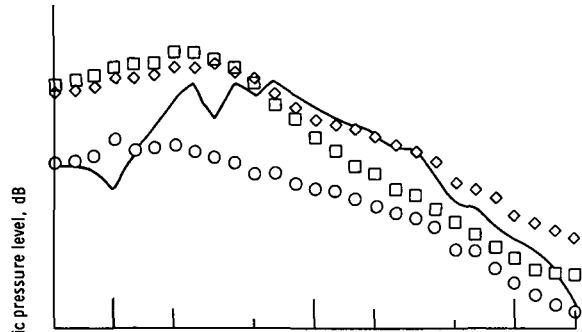


(b) Typical sound pressure level (SPL) spectra. Directivity angle, θ , 85°.

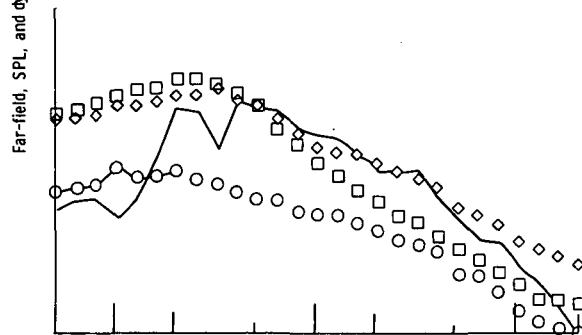
Figure 22. - Typical acoustic characteristics of externally blown flap, under-the-wing configurations with combined jet-flow-impingement-area screens and flap-trailing-edge ramp screens. Jet velocity, V_N , 228 meters per second.



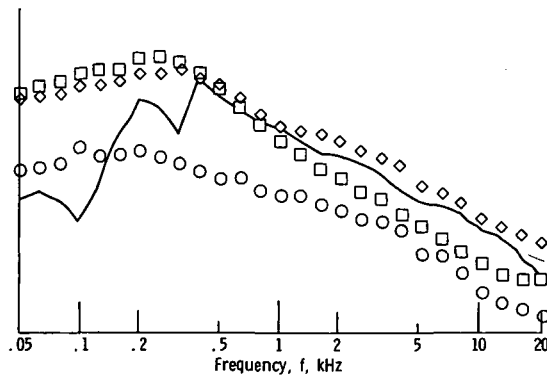
(a) Directivity angle, θ , 40° .



(b) Directivity angle, θ , 55° .

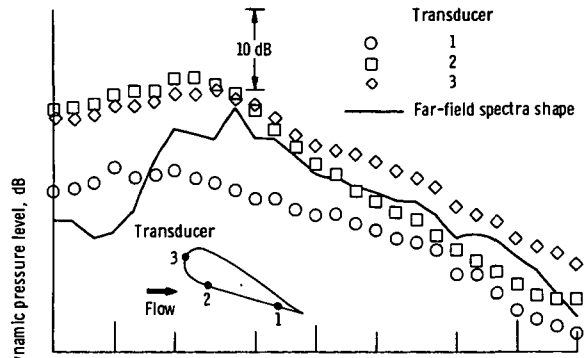


(c) Directivity angle, θ , 70° .

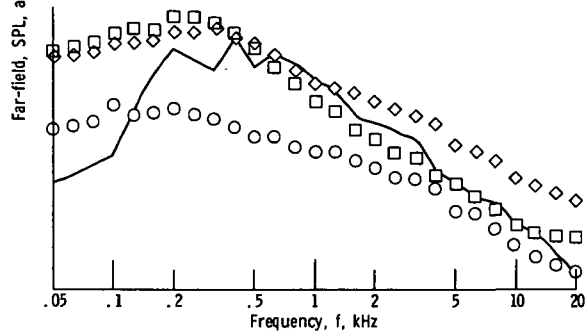


(d) Directivity angle, θ , 85° .

Figure 23. - Comparison of far-field and dynamic flap-surface pressure spectra for second flap with baseline hard-wall flap (configuration 2). Jet velocity, V_N , 228 meters per second.



(e) Directivity angle, θ , 100° .



(f) Directivity angle, θ , 155° .

Figure 23. - Concluded.



POSTMASTER: If Undeliverable (Section 158
Postal Manual) Do Not Return

"The aeronautical and space activities of the United States shall be conducted so as to contribute . . . to the expansion of human knowledge of phenomena in the atmosphere and space. The Administration shall provide for the widest practicable and appropriate dissemination of information concerning its activities and the results thereof."

—NATIONAL AERONAUTICS AND SPACE ACT OF 1958

NASA SCIENTIFIC AND TECHNICAL PUBLICATIONS

TECHNICAL REPORTS: Scientific and technical information considered important, complete, and a lasting contribution to existing knowledge.

TECHNICAL NOTES: Information less broad in scope but nevertheless of importance as a contribution to existing knowledge.

TECHNICAL MEMORANDUMS: Information receiving limited distribution because of preliminary data, security classification, or other reasons. Also includes conference proceedings with either limited or unlimited distribution.

CONTRACTOR REPORTS: Scientific and technical information generated under a NASA contract or grant and considered an important contribution to existing knowledge.

TECHNICAL TRANSLATIONS: Information published in a foreign language considered to merit NASA distribution in English.

SPECIAL PUBLICATIONS: Information derived from or of value to NASA activities. Publications include final reports of major projects, monographs, data compilations, handbooks, sourcebooks, and special bibliographies.

TECHNOLOGY UTILIZATION PUBLICATIONS: Information on technology used by NASA that may be of particular interest in commercial and other non-aerospace applications. Publications include Tech Briefs, Technology Utilization Reports and Technology Surveys.

Details on the availability of these publications may be obtained from:

SCIENTIFIC AND TECHNICAL INFORMATION OFFICE

NATIONAL AERONAUTICS AND SPACE ADMINISTRATION

Washington, D.C. 20546